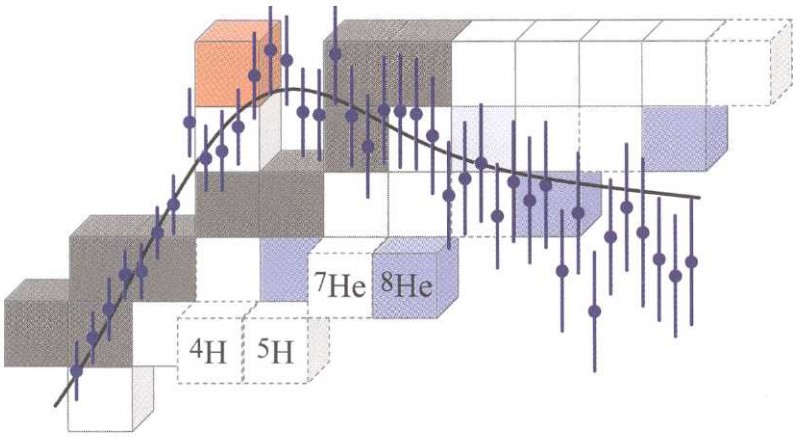

Teeter on the brink of nuclear stability

– Experimental investigations of very neutron rich light nuclear systems

MIKAEL MEISTER

Department of Experimental Physics
Chalmers University of Technology,
Göteborg University

CHALMERS | GÖTEBORG UNIVERSITY

CHALMERS | GÖTEBORG UNIVERSITY

Teeter on the brink of nuclear stability

– Experimental investigations of very neutron rich light nuclear systems

MIKAEL MEISTER

Akademisk avhandling som för avläggande av filosofie doktorsexamen i fysik vid Göteborgs universitet försvaras vid offentlig disputation den 6 juni, 2003, klockan 10.15 i Vasa A, Vera Sandbergs Allé 8, Göteborg. Avhandlingen försvaras på engelska.

Fakultetsopponent: Professor Juha Äystö,
Department of Physics,
University of Jyväskylä, Finland

Examinator: Professor Björn Jonson
Handledare: Bitr. Prof. Göran Nyman

Avhandlingen finns tillgänglig vid
Forskargruppen för subatomär fysik
Avdelningen för experimentell fysik
CHALMERS TEKNISKA HÖGSKOLA
GÖTEBORGS UNIVERSITET
SE-412 96 Göteborg

Teeter on the brink of nuclear stability

– Experimental investigations of very neutron rich light nuclear systems

MIKAEL MEISTER

Subatomic Physics Group
Department of Experimental Physics
Chalmers University of Technology and
Göteborg University

Abstract

Over the past decade, numerous experiments and theoretical investigations have been devoted to dripline nuclei of the lightest elements. Among these, the heavy helium isotopes, belonging to the group where nuclear halo structure was first observed, and the very neutron rich hydrogen isotopes believed to embody a similar structure, attracted much attention. This thesis concerns experimental studies of nuclei having excess neutrons, teetering on the brink of nuclear stability. More precisely, ^{8}He and its unbound subsystem ^{7}He and the two unbound hydrogen isotopes ^{4}H and ^{5}H are studied.

In a complete kinematics experiment performed at GSI, dissociation of 227 MeV/u ^{8}He in carbon and lead targets has been studied. From the data, the relative energy spectra and angular distributions, in the one-neutron knock-out channel ^{6}He+n, and in the diffractive dissociation and inelastic scattering channel into ^{6}He+2n, could be extracted. The data are compared with previously published results of ^{6}He and the unbound ^{5}He to illuminate the resemblances and differences of the corresponding nuclei, revealing a more complicated structure of the two heavier isotopes. In addition, the unbound hydrogen isotopes ^{4,5}H originating from the one-proton knock-out channel of 240 MeV/u ^{6}He in a carbon target have been studied. Relative energy spectra as well as energy and angular correlations in the t+n and t+n+n systems were investigated. The t+n+n relative energy spectrum is observed as a broad structure, peaked at 3 MeV above the threshold, and the two-body t+n system reveals a resonance compatible with earlier results for ^{4}H. In addition, analyzing the energy and angular correlations using the method of hyperspherical harmonic expansion allowed to determine the relative weights of the most relevant partial waves in the three-body t+n+n final state.

Keywords: ^{4}H, ^{5}H, ^{7}He, ^{8}He, angular distributions, breakup reactions, electromagnetic dissociation, exotic nuclei, relative energy spectra, energy and angular correlations, hyperspherical harmonics

Thesis for the degree of Doctor of Philosophy

Teeter on the brink of nuclear stability

– Experimental investigations of very neutron rich light nuclear systems

MIKAEL MEISTER

Subatomic Physics Group
Department of Experimental Physics
CHALMERS UNIVERSITY OF TECHNOLOGY
GÖTEBORG UNIVERSITY
Göteborg, Sweden 2003

Teeter on the brink of nuclear stability
– Experimental investigations of very neutron rich light nuclear systems
Mikael Meister
ISBN 91–628–5688–X

Subatomic Physics Group
Department of Experimental Physics
Chalmers University of Technology and Göteborg University
SE–412 96 Göteborg
Sweden
Telephone +46 (0)31–772 1000

Cover:
Excerpt of the nuclear chart for very light nuclei. Marked isotopes are the ones investigated in this work, see also Fig. 2.2. The data points illustrates the relative energy spectrum of the decaying t+n+n system, taken from Fig. 5.11.

Chalmers reproservice
Göteborg, Sweden 2003

Teeter on the brink of nuclear stability

– Experimental investigations of very neutron rich light nuclear systems

MIKAEL MEISTER

Subatomic Physics Group
Department of Experimental Physics
Chalmers University of Technology and
Göteborg University

Abstract

Over the past decade, numerous experiments and theoretical investigations have been devoted to dripline nuclei of the lightest elements. Among these, the heavy helium isotopes, belonging to the group where nuclear halo structure was first observed, and the very neutron rich hydrogen isotopes believed to embody a similar structure, attracted much attention. This thesis concerns experimental studies of nuclei having excess neutrons, teetering on the brink of nuclear stability. More precisely, ^{8}He and its unbound subsystem ^{7}He and the two unbound hydrogen isotopes ^{4}H and ^{5}H are studied.

In a complete kinematics experiment performed at GSI, dissociation of 227 MeV/u ^{8}He in carbon and lead targets has been studied. From the data, the relative energy spectra and angular distributions, in the one-neutron knock-out channel ^{6}He+n, and in the diffractive dissociation and inelastic scattering channel into ^{6}He+2n, could be extracted. The data are compared with previously published results of ^{6}He and the unbound ^{5}He to illuminate the resemblances and differences of the corresponding nuclei, revealing a more complicated structure of the two heavier isotopes. In addition, the unbound hydrogen isotopes ^{4,5}H originating from the one-proton knock-out channel of 240 MeV/u ^{6}He in a carbon target have been studied. Relative energy spectra as well as energy and angular correlations in the t+n and t+n+n systems were investigated. The t+n+n relative energy spectrum is observed as a broad structure, peaked at 3 MeV above the threshold, and the two-body t+n system reveals a resonance compatible with earlier results for ^{4}H. In addition, analyzing the energy and angular correlations using the method of hyperspherical harmonic expansion allowed to determine the relative weights of the most relevant partial waves in the three-body t+n+n final state.

Keywords: ^{4}H, ^{5}H, ^{7}He, ^{8}He, angular distributions, breakup reactions, electromagnetic dissociation, exotic nuclei, relative energy spectra, energy and angular correlations, hyperspherical harmonics

"anonymous" accelerator designers, operators, technicians, engineers, etc. The interaction among the people in the collaborations is substantial, and it is therefore often difficult to attribute ideas and results to a single person.

For those of you not wanting the read the entire thesis should know that the work is organized in the following way. Chapter 1 is written for a general audience who is interested in getting a taste and a brief introduction to the field of nuclear physics in general, and exotic nuclei in particular. While Chapter 1 only assumes a small physics knowledge, Chapter 2 goes further into detail, bringing us beyond the basics, emphasizing on nuclear structure studies at the dripline, providing additional background to the work that follows. Further, Chapters 3 and 4 concern experimental techniques and probes used to extract the information of interest. The Papers, and the experimental results, are discussed and summarized in Chapter 5, and to some extent also in Chapter 6 where I in addition evaluate the work from a more personal perspective. The end is devoted to a small Appendix closely related to to the analysis performed in Papers IV and V.

The work is written as an attempt to present the basic ideas together with a fair amount of background material. A casual reader should be aware that the writing at times is quite dense and interweaved. Further, I have made no special effort to give the impression that all details should be immediately understandable. Finally, the thesis is undoubtedly biased by my own limited understanding and prejudice, and even though the work is of restricted size I would like to apologize sincerely to all colleagues whose work has not been discussed or quoted adequately.

Mikael Meister

Göteborg, Sweden
May 2003

Contents

CHAPTER 1

Introduction

1.1 A brief history of time

The synthesis of elements began around one billion years after the big bang. Back then, the first galaxies and stars had formed from gigantic clouds of hydrogen. The gravitational energy thereby liberated, heated the stellar matter to such a degree that the process of nuclear fusion started at the core of these newly born stars. The result was the synthesis of helium from hydrogen. Since then complex nuclear reactions within stars have been responsible for the synthesis of elements.

Human life, too, arose as a result of such processes. For just like all the matter around us, each and every atom in our bodies originated as dust from stars of earlier generations.

There have been times when natural philosophers believed that they understood the ultimate structure of matter – that they knew the fundamental building blocks of which everything is made. The followers of Aristotle thought as much when they argued that everything is made up of various portions of the four elements, earth, air, fire, and water. However, by the late Middle Ages, this simple picture had been complicated by the addition of quicksilver (mercury), sulphur, and a number of other substances, and the continual addition of more elements to the list led to its abandonment. If there are too many kinds of building blocks, it is hard to believe that they are fundamental.

In the early days of modern chemistry (about 1800), a similar hope rose. But in the course of the nineteenth century, the number of elements grew to almost one hundred – again too many to be regarded as truly fundamental.

With the discovery of the structure of the atom in the first few decades of the twentieth century, the hope rose again. By 1920 or so, it was plausible to argue that all matter was built up of protons and electrons, with photons acting as the carriers of electromagnetic energy. Things became a little more complicated with the discovery or postulation in the early 1930s of the neutron, the neutrino, the positron, and a few other particles. This period is often referred to as the early childhood of nuclear physics and during these years, and shortly after, great theoretical progress on the nature of nuclear forces and the development of simple nuclear models (liquid-drop model, shell model, collective model) were accomplished [1]. Many characteristics of ground-state nuclei, like their masses, spins, magnetic moments and decays where systematically investigated, and the discovery of nuclear fission and its first technical applications gained nuclear physics wide acclaim.

The fact that we now rather well understand nuclei in the vicinity of the valley of stability does not mean that we have a complete picture of the complicated many–body system that constitutes an atomic nucleus.

1.2 Units, dimensions, structures

The lightest atom, hydrogen, has one proton and therefore one electron and the heaviest naturally occurring atom, uranium, has 92 protons and thus 92 electrons. In a rough sense this is all there is to the diversity of the chemical elements*, however to explain the stability of the elements we must also take into account the neutron number of each nucleus. This value can vary considerably for the nuclei of a given element, with a fixed proton number. The nucleus of ordinary hydrogen has e.g. one proton and no neutrons, the latter fact making it unique among all nuclei. But a hydrogen nucleus can also exist in a form that has one proton and one neutron. This nucleus is called a deuteron, and the atom still with only one electron is called deuterium. Chemically it is still hydrogen as is also the heavier radioactive form tritium, which has one proton and two neutrons. A tritium nucleus is called a triton. These separate nuclei of a single chemical element, differing only in neutron number, are the isotopes of that element. Although the chemical properties of the isotopes of a given element are the same, their nuclear properties can be very different.

*The element is defined by the number of electrons surrounding the nucleus.

To be more precise, the nucleus is characterized by its integer number of protons, Z (the atomic number) which uniquely specifies an element, and its number of neutrons, N, and of the total nucleon (mass) number, $A = Z + N$. Nuclei having the same Z, but differing in N, are called *isotopes*; those having the same N, but differing in Z are called *isotones*. Nuclei having the same nucleon number A are termed *isobars*. The simplest nomenclature of a nucleus is that given by its chemical symbol, with the nucleon number A as a superscript to the left. Which means that ^{12}C denotes a carbon nucleus ($Z = 6$) with mass number $A = 12$ and neutron number $N = 6$. The carbon isotope having 8 neutrons is then denoted ^{14}C. The naturally occurring elements thus cover a range from $Z = 1$ to $Z = 92$, whereas elements with atomic numbers up to $Z = 116$ [2] have been created in laboratories.

Further, in nuclear physics we encounter lengths in the order of 10^{-15} m, which is called one femtometer (fm). This unit is quite often referred to one fermi, to honor the pioneer nuclear physicist Enrico Fermi. Nuclear sizes range from about 1 fm for a single nucleon to about 7 fm for the heaviest nuclei.

The time scale of nuclear phenomena has an enormous range. Some nuclei such as e.g. ^{5}He and ^{11}N break apart in times of the order of 10^{-20}s [3, 4]. Many nuclear reactions take place on this time scale, which is roughly the length of time that the reacting nuclei are within range of each other's nuclear forces. Electromagnetic transitions in nuclei occur generally within lifetimes of the order $10^{-9} - 10^{-12}$s. However, radioactive decays can occur with much longer *or* shorter lifetimes, α and β decays e.g. often appear with lifetimes in the order of minutes or hours, but sometimes thousands or even millions of years.

Nuclear energies are conveniently measured in millions of electron volts (MeV), where 1 eV $= 1.602 \cdot 10^{-19}$ J is the energy by a single unit of electronic charge when accelerated through a potential difference of one volt. Further, nuclear masses are measured in terms of atomic mass units, u, defined so that the mass of an atom of ^{12}C is exactly 12u. Nuclear physicists rather work with mass energies than masses themselves. The conversion factor is 1 u = 931.502 MeV, using the fundamental result from special relativity $E = mc^2$ makes it possible to work either with energies or masses, where $c^2 = 931.502$ MeV/u in these units.[†]

[†]For the entity "energy per nucleon" the units MeV/u are used throughout the thesis. This is not a strictly correct notation, but it is very commonly used instead of MeV/nucleon.

1.3 The nuclear landscape

Nuclei are complex quantal systems with a finite number of particles, and their binding energies[‡] determined by the interplay between the strong and the electromagnetic interaction.

At low energies, the nuclear properties are described in terms of nucleons and virtual mesons, with empirically deduced effective interactions between them. Information on these properties is derived from nuclear structure studies using advanced spectroscopic tools. At high energies, the substructure of nucleons and mesons in terms of quarks and gluons becomes visible. The strong interaction between these fundamental building blocks of matter is described by quantum chromodynamics (QCD). Theories of strings, super symmetries and M-theories try to describe quarks, electrons and other subatomic particles in terms of even more fundamental building blocks. An interesting and popular account of the latest developments in this area can be found in [5].

Nuclear physics has many links to particle– and astrophysics and modern research in these fields is closely related to the various phases in the evolution of the Universe. The experiments to detect the quark gluon plasma, to study the abundance of the lightest elements, the attempts to model the production of heavy nuclei and to determine the equation of state of nuclear matter, the search for neutrino masses and dark matter are all shared by nuclear physics, particle physics and astrophysics.

Taking a closer look at the area of interest for a nuclear scientist, Fig. 1.1 shows a map of the nuclear landscape. Today we believe there can only exist a limited number of nuclei, of these about half have already been seen in the laboratory but only a small number exist naturally on Earth, these are marked by black squares and defines the valley of β–stability. Nuclei to the left of the valley are unstable against β^+–decay or electron capture, and nuclei to the right are unstable against β^-–decay. Nuclides heavier that ^{209}Bi are all unstable, and decay mostly by α–decay or in some cases spontaneous fission. The only heavy nuclides with sufficiently long half-lives to still be found on Earth are ^{232}Th and ^{234,235,238}U. The size of a nucleus, and therefore also the upper right boundary of the chart is limited due to fission and the exact location of this limitation is not yet known. Experiments trying to synthesize super–heavy elements are eagerly exploring this limit.

[‡]The binding energy B of a nucleus is the difference in mass energy between a nucleus ${}^{A}_{Z}X_N$ and its constituent Z protons and N neutrons : $B = \{Zm_p + Nm_n - [m({}^{A}X) - Zm_e]\}c^2$ if the electron binding energies are neglected, m_p, m_n, m_e are the masses of the proton, neutron and electron respectively and $m({}^{X}A)$ is the atomic mass.

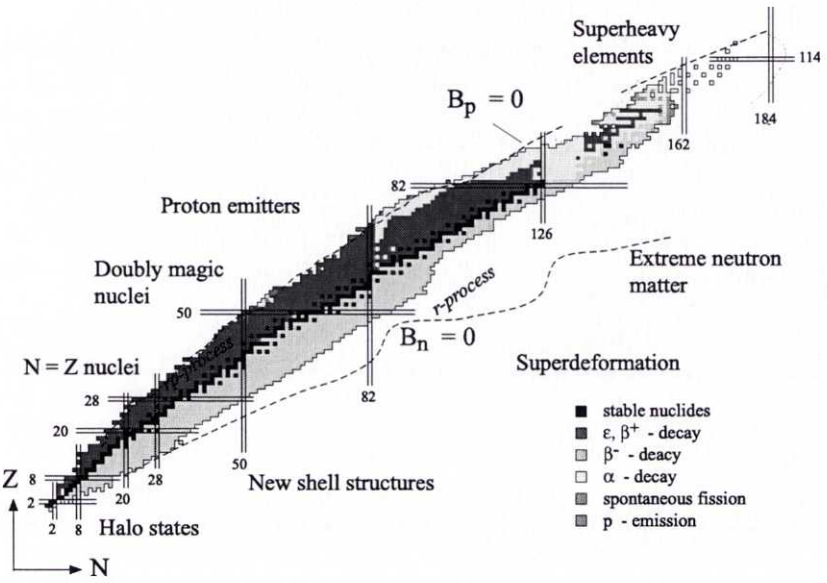

Figure 1.1: *Map of the nuclear landscape.*

The so called magic numbers which are associated with increased stability are usually convenient "landmarks" and are indicated by double lines in the map. The variation of the neutron-to-proton ratio on both sides of the valley of β–stability leads to a loss of binding energy of the last nucleon when approaching the borderlines of stability, the *driplines*, where the next proton or neutron respectively is not bound any more ($B_{n,p} = 0$). The driplines in the figure are only estimates, and especially, the exact location of the neutron dripline is not well known.

The number of primordial nuclei is less than 300 (the number depends on how stability is defined), while almost 6000 nuclei are supposed to "exist" in the sense that they live much longer than the time it takes a nucleon with an energy about 5–8 MeV to cross the nucleus ($\tau \sim 10^{-22}$ s)[§]. Only about half of these supposedly existing ones have been observed up to now. While the proton dripline is reached or almost reached over a large mass range, the neutron drip line is only reached for the lightest elements, due to difficulties to produce the extreme neutron rich nuclei experimentally.

[§]This is also referred to as the Fermi velocity of the nucleon.

Figure 1.1 also shows the nuclei involved in the r– and rp–process [6], which are important scenarios responsible for the production of nuclides in the Universe. A third path, not shown in the figure is the s–process which runs along the stable nuclei. Many of these astrophysical scenarios are unfortunately still quite poorly understood, again mainly because the properties of the nuclei involved, are not yet known experimentally.

Another noticeable phenomenon in the nuclear landscape is proton emission. The forces between the nucleons in a nucleus can be approximated by a nuclear potential, and since neutrons and protons are both Fermions, each of them can only occupy one state due to the Pauli principle. In this way, they fill the potential well up to the Fermi level, but due to the repulsive Coulomb force between the protons, the well seen by the protons is less deep, and in addition the long–range Coulomb force creates a Coulomb barrier.

In the valley of β–stability, the Fermi levels of protons and neutrons are almost equal. When for example adding more neutrons to a nucleus it leads to a higher Fermi level for the neutrons, and when reaching the neutron dripline, the Fermi level for the neutrons is situated at zero energy. Therefore, nuclei beyond the neutron dripline cannot exist, since the excess neutrons would leave the nucleus immediately. At the proton dripline, using the same reasoning, the Fermi level for the protons is thus also situated at zero energy. However, nuclei beyond the proton dripline may exist as very narrow resonances, because the excess protons must first tunnel through the Coulomb barrier before they can leave. Therefore, if tunneling of protons is comparable, or faster than β–decay, spontaneous emission of protons is observed.

An interesting consequence of the Coulomb force is the curvature of the valley of β–stability, which easily can be seen in the figure.

One key feature of nuclear structure, which is of great importance to the universe as we know it, is the absence of stable five or eight-body nuclei, see Fig. 2.2. This simple fact is crucial to both primordial and stellar nucleosynthesis. It leads to a universe whose baryonic content is dominated by hydrogen and ^{4}He, with trace amount of deuterium, ^{3}He, and ^{7}Li. It also enables stars such as our sun to burn steadily for billions of years, allowing time for the evolution of life intelligent enough to wonder about such issues.

CHAPTER 2

Light and very neutron rich nuclei

As previously mentioned nuclear stability is determined through the interplay of the attractive nucleon–nucleon strong force and the repulsive Coulomb force. An intriguing problem is what happens to the nuclear matter as the limits of stability are approached. Many of these areas of the chart of nuclides have only recently been opened for experiments, and a great number of exciting phenomena have already been discovered.

The essential element, resulting from basic quantum mechanics involved while studying one–dimensional radial problems of quantum systems moving in short range spherical potentials, is that the wave functions behave asymptotically as exponential functions, given by the expression:

$$\psi(r) \propto \exp(-\kappa r), \tag{2.1}$$

with $\kappa = (2m|E|)^{1/2}/\hbar$, and $|E|$ the binding energy (E < 0). This allows particles to move far away from the center of the attractive potential when E approaches zero. This idea can be extended easily to more realistic and complex systems but the essentials remain: particles, e.g. neutrons can move out into the classical "forbidden" region of space. This has given rise to the subsequent observation of neutron "halo" system in weakly bound nuclei where a new organization of protons and neutrons takes place which minimizes the energy by maximizing the coordinate space available.

2.1 Halo nuclei

Less than two decades ago experiments carried out by Tanihata and coworkers at Berkeley [7], enabled them to extract the interaction radii of light nuclei from interaction cross section measurements (the interaction cross section is here defined as the total reaction cross section if the nucleus has no bound state, i.e. for all reaction channels where the proton and/or neutron number is changed in the interaction). The real surprise was to observe significantly larger matter radii in nuclei like ^{6,8}He and ^{11}Li compared to more typical p–shell nuclei with a radius of about 2.5 fm. The data is shown in Fig. 2.1 together with the $r = r_0 \cdot A^{1/3}$ behavior, with $r_0 = 1.2$ fm (today, these values have however been recalculated, including correlations in the projectile nuclei implied by their effective few body character, see for example Ref. [8]). The results clearly pointed out that nuclear matter is more extended than normally assumed, forming halo–like structures. It was realized that the charge distribution in such neutron rich nuclei could be determined by measuring electric quadrupole moments. Experiments carried out at ISOLDE [9] unambiguously showed that the charge distribution of ^{11}Li is almost identical to the charge distribution in ^{9}Li thus bringing in additional and clear evidence that the large matter radii obtained were due to some unexpected behavior of the last two neutrons, forming a halo structure around the ^{9}Li core. The

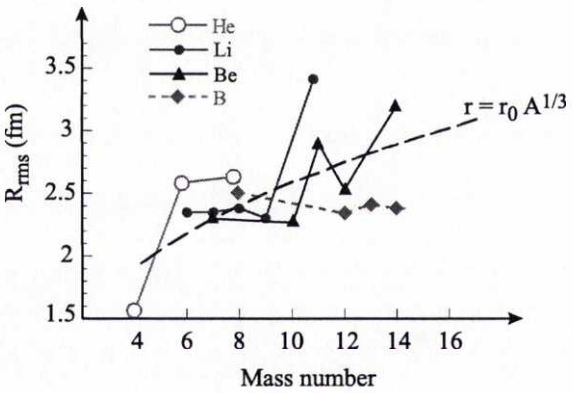

Figure 2.1: *Schematic illustration of interaction radii for light nuclei determined from interaction cross sections. A sudden increase of the matter radii is observed for a number of nuclei near the neutron drip line. The radii are deduced from Refs. [7, 10, 11] using Glauber theory.*

findings by Tanihata et al. inspired P. G. Hansen and B. Jonson to develop a simple model in order to describe this behavior [12]. A calculation in analogy to what can be made for the loosely bound deuteron was made, substituting the proton with a ^{9}Li core and the neutron with the two remaining neutrons (assuming a di-neutron). With a two neutron separation energy of only 295 keV, the di-neutron wave function spends as much as 80% of the time outside the nuclear potential. There is no strict definition of a halo, but some authors [13, 14] define a state as a halo when the halo–nucleon wave function spends more than 50% of the time in the forbidden region.

Present day experiments probe not only global features of halos like cross sections, but also structural details, such as spectroscopic factors and weights of wavefunction components. The arsenal of experimental tools include momentum distribution measurements, γ-ray experiments, complete kinematics break-up measurements and β-decay studies, of which some will be discussed in subsequent sections.

Some of the properties characterizing a halo nucleus is:

- The most outstanding property is the small separation energy of the last bound nucleon(s). In an ordinary nucleus the separation energy is about 8 MeV, while in a halo nucleus it is usually less than 1 MeV.

- As a consequence of the Heisenberg uncertainty principle an extended halo nucleon wavefunction implies a narrow momentum distribution according to
$$\overline{(\Delta x)^2(\Delta p)^2} \geq \hbar^2/4. \tag{2.2}$$
For more tightly bound nuclei, the momentum distribution of fragments after breakup is broader due to a more confined nuclear volume.

- The interaction cross section is large in comparison with neighboring nuclei, this due to the extended r.m.s. matter radius that exceeds the $r_0 = A^{1/3}$ dependence of nuclei closer to stability.

- The halo state should have a low relative momentum barrier to allow the halo nucleon(s) to tunnel out beyond the reach of the strong force, most preferably s- or p-wave neutrons. The size of a proton halo has the be smaller than its neutron counterpart due to the additional Coulomb barrier which hinders its formation.

- A large Coulomb dissociation cross section characterizes the halo nuclei. The loosely bound neutrons are easily separated from the core by the virtual photon field created in the Coulomb scattering process.

- A special feature of the two-neutron halo nuclei is that no bound subsystems are believed to exist, such a structure is usually referred to as a Borromean system [15]. (Note however the recent paper [16], where a possible non Borromean two neutron halo in ^{16}C is discussed.)

Ever since the first discoveries the field has grown enormously and a thorough examination, both experimentally and theoretically, of the halo concept (and also for more complex systems or nuclei with external neutron rich skins) can be found in some highly readable papers [15, 17–21]. In these articles, extensive references are given to the recent but already very large set of results in this field.

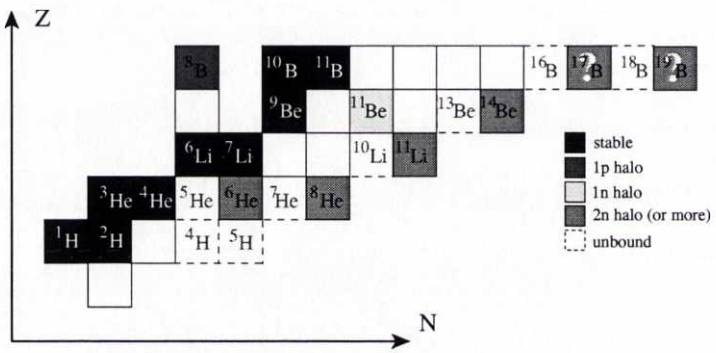

Figure 2.2: *Excerpt of the nuclear chart for very light nuclei. Known and suggested halo nuclei are marked as indicated in the figure. White fields are β-decaying isotopes.*

2.2 The Helium isotopes

Looking at Fig. 2.2 the jagged edge of the neutron dripline is very striking. It demonstrates another structural feature of dripline nuclei i.e. the importance of pairing in loosely bound systems. This quality is most remarkable for the helium isotopes. Trying to add one neutron to ^{4}He will fail since ^{5}He is unbound. However, adding two neutrons to the α–particle will form ^{6}He, which is a bound (very loosely, but nevertheless bound) two neutron halo nucleus. Continue towards the neutron dripline, the story repeats itself with ^{7}He and ^{8}He, where ^{8}He has a very special structure which will be discussed

in detail in Chapter 5. Continuing even further we reach ^{9}He and the doubly magic ^{10}He which both have been quite extensively investigated during the last years [22–28]. One particular important question when reaching regions far beyond the neutron dripline is whether the N = 8 remains a magic number or not depending on the strength of the LS force, see e.g. Refs. [29–32].

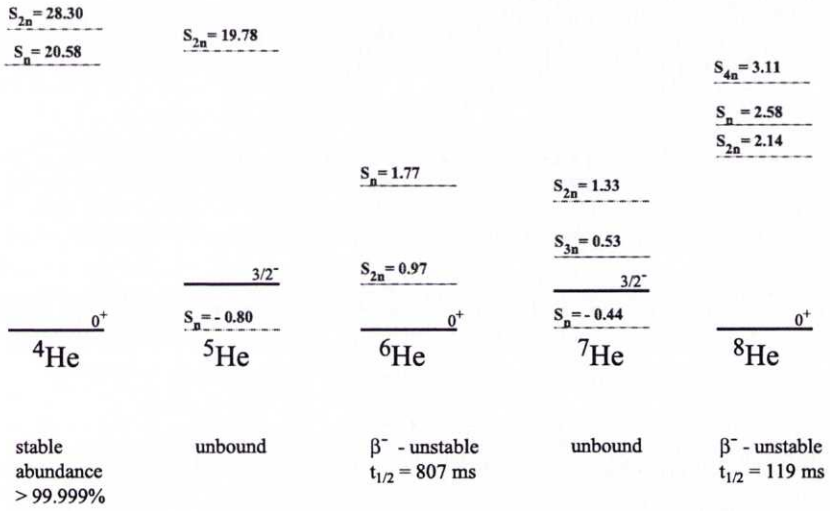

Figure 2.3: *Schematic overview of separation energies in helium isotopes, energies are in MeV but the scale is arbitrary, data taken from [33, 34].*

The helium isotopes play a specific role in the concept of halo physics, mainly due to the fact that their structure may be described as a tightly bound ^{4}He core surrounded by a number of neutrons. This "core + valence neutron" structure is the basis of a model [15] introduced to explain the halo structure of ^{6}He [20, 21] and the five-body cluster structure of ^{8}He [35–37]. The nuclides ^{5}He and ^{7}He are unbound and have ground state spins $I^{\pi} = 3/2^{-}$ [34], corresponding to a neutron in a $p_{3/2}$ orbital according to the standard shell-model.

The stability (with respect to particle decay) of the A=8 isobar chain terminates on the neutron-rich side with ^{8}He. This nucleus has the largest N/Z ratio for any known particle-stable nuclear system. The lighter isotope ^{6}He is characterized as a Borromean two-neutron halo system [15] and has been

studied in a large number of different experiments. Its structure is well understood and the ground state is to more than 90% a pure $(0p_{3/2})^2$ state [38]. The relatively simple structure of ^{6}He makes it a bench-mark nucleus which can be used for comparative studies of nuclei close-by. The separation energy of the neutron pair in the $0p_{3/2}$ shell, forming the halo in ^{6}He, amounts to 973 keV while 2.139 MeV is needed to remove a neutron pair in ^{8}He. The neutron pairing energy in ^{8}He ($\epsilon = 3.03$ MeV) is one of the largest known and it is 275 keV larger than that of ^{6}He. A careful analysis of the measured cross sections for different breakup channels of ^{6}He and ^{8}He [39] suggests that the ^{8}He structure is best described as a five body system $(\alpha + 4n)$ rather than as a two-neutron halo (^{6}He+$2n$). Further experimental evidence for an α-neutron structure has been obtained in beta-decay experiments [40] where the beta-delayed triton branch mainly originates from a 9.3 MeV resonance in ^{8}Li, and has a GT (Gamow–Teller) reduced transition rate of $B_{GT} = 5.18$ corresponding to almost half of the GT sum rule strength [41]. This result indicates that the ^{8}He ground state has a large overlap with an (α+t+n) structure in ^{8}Li [42]. Zhukov et al. [35, 43] have suggested a five-body cluster orbital shell model approximation (based on the discussion in Ref. [44]) to describe the ^{8}He ground state wave function as $(\alpha + 4n)$.

2.2.1 Helium analomy

The semiempirical massformula*, suggests that the binding energy of the last neutron in the nucleus should decrease smoothly with increasing number of neutrons [46]. However, due to nucleon pairing and shell effects which cause discontinuities in the resulting monotonic behavior, this dependence should be treated separately for nuclei with even and odd number of neutrons. Excluding these effects though, a universal dependence appears; stability always decreases with the addition of one pair of neutrons. An increase of the neutron binding energy is rarely observed, and the strongest stability increase with number of neutrons is observed for the ^{6}He -^{8}He pair, where it exceeds 1 MeV. Further, consider the binding energies of the odd He isotopes. In the transition from ^{5}He to ^{9}He, i.e. an addition of four neutrons, the binding energy does not effectively change, according to some authors there might even be an increase, see Fig. 2.4. This effect is usually referred to as "Helium analomy" [47].

*Originally developed by Weizäcker, Bethe and Bacher [1, 45].

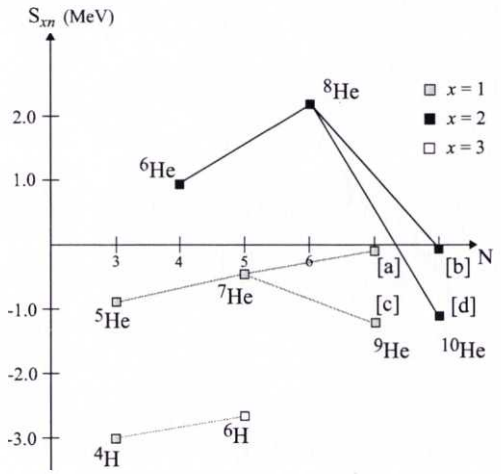

Figure 2.4: *Systematics of the binding energy with respect to the first particle threshold, S_{xn} for H and He isotopes, error bars excluded [34]. Data for [a-d] are taken from Refs. [25, 27, 48, 49] respectively. The connecting lines are only guides for the eye.*

Until now no microscopical explanation of this unusual stability of the heavy helium isotopes is available, and the question whether it is a reflection of the large neutron excess compared to more conventional nuclei or if this is a qualitatively new phenomena is not clear. Presently it is not possible to experimentally test any hypothesis on other nuclei. The only pair of nuclei[†] with fairly known masses having a very large neutron excess are the heavy unstable hydrogen isotopes, ^{4}H and ^{6}H (for these isotopes the experimental data are quite consistent [33, 34]). Their decay energies (with respect to one and three neutrons) are also given in Fig. 2.4. Even though the errors are rather large, a trend similar to that of the He isotopes is observed, i.e. when adding two neutrons to ^{4}H forming ^{6}H the instability does not seem to increase.

Presently there are no experimental data on heavier helium isotopes. A very rough estimation though (since no experimental data for ^{13}Li exist) along the $N = 10$ isotone, would result in a system unbound by approximately 2-3 MeV for ^{12}He.

[†]The word nuclei (or isotopes) will be used hereafter for simplicity, even though these unbound systems might be better referred to as resonances.

2.3 Hydrogen

Some decades ago it was suggested that the ^{5}H nucleus might be situated near the breakup threshold and even be stable [50]. A lower limit on the mass of ^{5}H was obtained a few years later [51] from the absence of sharp structures in the ^{3}He(^{3}He,n)^{5}Be reaction up to 4.2 MeV. Since then the studies of the heavy hydrogen isotopes (3<A<8) have been given much attention and lately some intriguing results have been reported. The structure of a heavy hydrogen nucleus is expected to be similar to that of neutron-rich helium isotopes, namely, an inert core surrounded by valence neutrons [47, 52, 53]. The ^{5}H isotope, with an even neutron number, could be less unbound than ^{6}H or even ^{4}H due to the neutron pairing energy. However, the width of this state, estimated in a conventional R-matrix approach is extremely large (10-15 MeV) due to the absence of Coulomb and centrifugal barriers in the $t+$ di-neutron channel [47, 52]. Below some considerations will be formulated allowing such a large width to be understood qualitatively, even though the decay energy is comparatively low. For the isotopes with odd number of neutrons (^{4}H and ^{6}H), the experimental studies have however revealed their ground states as comparatively narrow resonance states situated 2-3 MeV above the dissociation threshold [33, 34]. The experiments aiming at an identification of ^{5}H have however given extremely contradictory results [34, 54–56], without any safe assignment of neither the resonance position nor its width. Estimations of the width have been in a broad span from less than 500 keV up to more that 10 MeV.

2.3.1 Nuclear systems with even number of neutrons

An interesting fact when studying the systematics of unbound neutron rich nuclei is that systems with an even number of neutrons such as a possible ^{4}n, ^{5}H and ^{7}H are more difficult to produce and detect than those with odd neutron number (note however the very recent publications by Marqués et al. [57] and Korsheninnikov et al. [56, 58]). At a first glance this seems strange, because due to nucleon pairing energy, nuclei with an even number of neutrons are quite often more stable than nuclei with an odd number of neutrons.

It may turn out that the decay energy of the above mentioned nuclear systems is high, leading to a large width. However it might be reasonable to assume that a specific effect takes place which, even if the decay energy is low, results in an unobservably large width. Following the ideas of Goldansky [59]

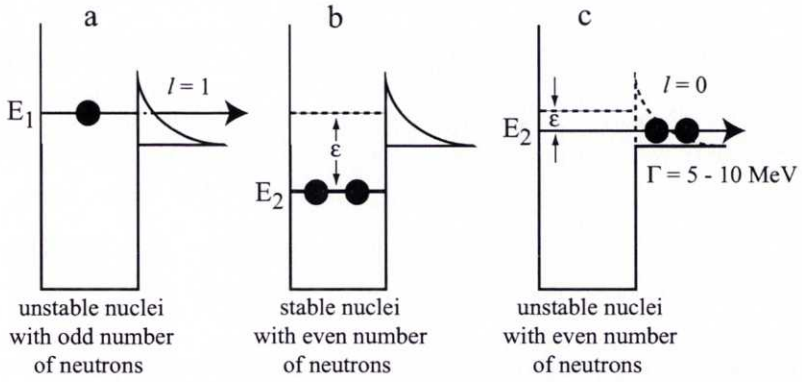

Figure 2.5: *Schematic representation of the centrifugal barrier influence on the decay with odd and even number of neutrons in $l = 1$ states. (a) One neutron subdues the centrifugal barrier. (b) When a neutron is added to make an even number, the pairing energy is high enough and the system is bound. (c) When a neutron is added to make an even number, the system is unbound, and decays by two neutron emission. After pairing a di-neutron may appear with $l = 0$ relative to the residual nucleus and the decay can take place without penetration through the centrifugal barrier.*

about two proton emission[‡] it was assumed [62] that the pairing effect of two nucleons forming a di-nucleon, having zero angular momentum with respect to the residual nucleus, allows emission in the absence of a centrifugal barrier.

Consider a nucleon in a quasi-stationary state E_1, blocked by the centrifugal barrier, see Fig. 2.5. The addition of a second nucleon will change the energy of this state, which becomes approximately equal to

$$E_2 = 2E_1 - \varepsilon, \tag{2.3}$$

where ε is the pairing energy, and will result in either of two possible situations. If the energy gain due to pairing is high enough, the resulting new two-nucleon state becomes a bound state, and the even (with respect to neutrons) nucleus will be stable. This effect is e.g. observed in the transitions

[‡]For recent theoretical investigations of two proton emission see Refs. [60, 61].

from ^{5}He to ^{6}He and ^{7}He to ^{8}He. However, another situation is also possible, in which the energy gain due to pairing is not sufficient to bind the system and the two-nucleon state will remain unbound. The formed nucleus will then be susceptible to many-particle (in the simplest case, a three-particle) decay. This situation could happen in the transitions from ^{4}H to ^{5}H, from ^{6}H to ^{7}H and as well from ^{9}He to ^{10}He. Which ever of the two possibilities is preferable depends on many parameters such as the position of the single-particle level, the pairing energy, the decrease in well depth due to the increase in neutron excess etc. that is a quite complex problem.

In this thesis, recent results from an experiment performed at GSI, Darmstadt concerning breakup of ^{6}He at 240 MeV/u and ^{8}He at 227 MeV/u in carbon and lead targets will be presented. This will hopefully shed some new light on the many questions concerning the very neutron rich hydrogen isotopes and heavy helium isotopes, teetering on the brink of nuclear stability.

CHAPTER 3

Experimental tools

High and medium energy physics research have always been the driving force behind the development of particle accelerators. Even though the early childhood of nuclear and particle physics started their lives in research laboratories in glass envelopes sealed with varnish and putty using electrodes and frequent discharges, they have long since outgrown this environment to become large-scale facilities offering services to large communities.

It was in the early twenties that the need for particle accelerators was first realized by Ernest Rutherford amongst others, but the electrostatic machines then available where far from reaching the necessary voltage and for a few years there was no advance. Suddenly the situation changed in 1928 when Gurney and Gamov independently predicted tunneling [63, 64] and it appeared that an energy of 500 keV might just be enough to split the atom. This seemed technologically feasible to Rutherford and he immediately encourage Cockcroft and Walton to start designing a 500 keV particle accelerator. Four years later in 1932, they split the lithium atom with 400 keV protons. This was the first fully man-controlled splitting of the atom [65] which later earned them the Nobel prize in 1951, *"for their pioneer work on the transmutation of atomic nuclei by artificially accelerated atomic particles"*, see [66] for further reading. Many of the exotic discoveries through the decades to come had not been possible without the development of radioactive ion beams (RIB) at different accelerator facilities around the world.

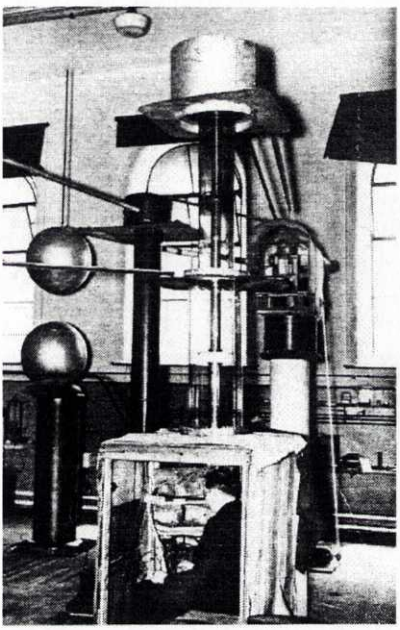

Figure 3.1: *A photograph of the Cockcroft-Walton accelerator installation at the Cavendish Laboratory. (From Lawrence and the cyclotron: AIP History Center Web Exhibit [67].)*

3.1 Production of radioactive nuclei

Study radioactive species requires production in the laboratory. Today, there are two main methods to produce radioactive beams, both with some modifications.

The IFS (In-Flight Separation) method, used at GANIL, GSI, MSU and RIKEN amongst other places, which uses high-energy heavy-ion fragmentation of stable nuclei, and the ISOL (Isotope Separator On Line) method, used for example at CERN–ISOLDE, Jyväskylä, Louvain-la-Neuve and SPIRAL at GANIL, where stopped target fragments are re-accelerated. The former technique provides fast, clean separation independent of the chemical element while the latter is superior in terms of beam intensity and geometrical beam quality. The two techniques address two different energy regimes with a very small overlap, and the different beam properties make the two techniques complementary, and different types of experiments are performed at facilities using IFS and ISOL. A general review over methods to produce RIB can be found e.g. in Refs. [68–71] and a popular review is found in [72].

3.1.1 In-Flight Separation (IFS)

In-flight separation is successful in producing intermediate and high energy beams above 50 MeV/u, where the radioactive ions are produced by fragmentation reactions of stable beams on stable targets. A first generation of IFS facilities is in operation at various laboratories in Europe, the USA and in Japan. Among these GSI is playing an important role, since it is the only facility worldwide, where beams of all elements are available with energies up to and about 1 GeV/u.

Mainly two types of fragmentation reactions can be considered, namely peripheral and central. The most neutron rich fragments are generally produced in peripheral collisions, while central collisions occurring at small impact parameters rather tend to produce a high multiplicity of fragments. The reaction products can range from individual nucleons to almost the mass of the beam particle, many of which will be produced at high excitations and will undergo subsequent γ or particle decays. It is therefore necessary to filter the secondary beam to increase the relative abundance of the species of interest.

The time of the separation process is determined by the time-of-flight through the spectrometer which is in the order of μs or less. Thus, the intensity of the secondary beam is usually not limited by the radioactive decay since the half lives of most isotopes of interest produced by fragmentation are appreciably larger.

Breakup reactions and Coulomb excitation of giant resonances are some examples of experiments well suited for this technique.

3.1.2 Isotope Separator On Line (ISOL)

The ISOL method which was the first to be developed [73], uses the radioactive ions produced by high-energy beams from a primary accelerator or neutrons from a nuclear reactor.

So far the highest intensities have been reached using high energy protons (at ISOLDE 1.4 GeV protons from the PS booster is used) which produce the radioactive isotopes through spallation, fission and fragmentation reactions in a thick target. At high temperatures the reaction products diffuse to the target surface, desorbe and effuse via a transferline into an ion source. After extraction and acceleration from the ion source, a magnetic separator system purifies the the beam, which can then be sent to experimental areas.

Depending on the selectivity of the target and ion source, the beams are often quite pure and the separator systems are not as complicated as in an

IFS facility, where the separator really creates the secondary beam out of a collection of fragments. However due to the rather slow diffusion processes, the lifetimes of the accelerated radioisotopes are limited downwards to a few ms, depending on the chemical and solid-state characteristics [74] of the reaction products. In this way it is possible to produce radioactive ion beams with low energies around and below the Coulomb barrier, typically 10-100 keV. The low energy beams can easily be implanted in thin foils and their decay properties can be investigated. The method has proven to be very useful, especially for reproducing astrophysical reactions which occur at these low energies, as well as for β–decay studies of halo nuclei [75, 76].

At many new facilities, such as SPIRAL and REX-ISOLDE, post accelerators are installed, see e.g. [77], where the secondary beams have energies ranging from one up to tens of MeV.

3.2 GSI

More than 30 years ago, on December 17, 1969, Gesellschaft für Schwerionenforschung (GSI) was founded, and its first beam was delivered in 1975. GSI [78] is a heavy ion research center funded by the Federal Government of Germany and the state of Hessen, and is located in a northern suburb of Darmstadt, approximately 25 km south of Frankfurt.

The present accelerator complex, consisting of the UNIversal Linear Accelerator [79] (UNILAC, beam energy of 2 - 20 MeV/u), the 60 meter diameter synchrotron for heavy ions [80] (SchwerIonenSynchrotron or simply SIS, 1 - 2 GeV/u), the FRagment Separator [81, 82] (FRS) and the Experimental Storage Ring [83] (ESR), permits acceleration of ions up to a maximum energy of 1000 to 2000 MeV/u for ion optical transfer to more than 30 different experimental set–ups.

Approximately 700 people are employed at GSI, including 300 scientists and engineers. The facility is open to national and international research groups, and more than 1000 scientists from over 25 countries are involved in the ongoing research activities pursued at GSI. The program covers a very broad spectrum, ranging from fundamental research in nuclear, atomic and bio physics as well as research in applied fields such as material sciences, plasma physics, cancer therapy, and accelerator development.

GSI is probably most famous for the discovery of the (super) heavy elements with atomic numbers 110, 111 and 112 [84] (resulting in the naming of the elements 108 and 110, hassium, Hs, and darmstadtium, Ds, respectively) and this research is still very much alive today searching for heavier elements.

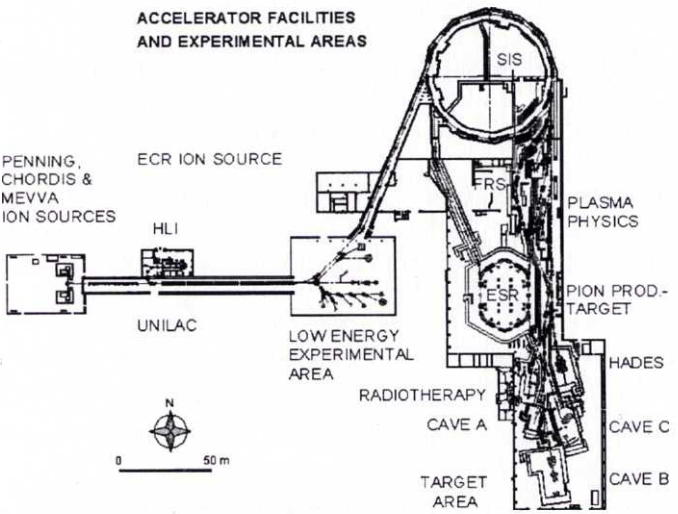

Figure 3.2: *A layout of the GSI accelerator facility.*

However today, GSI is probably equally famous for its cancer therapy, which has proven to be very successful in the treatment of human brain tumors [85]. Below follows a a brief summary of the ongoing research at GSI.

Nuclear and Hadron Physics

- Nuclear reactions up to relativistic energies.
- Equation of state for nuclear matter.
- Investigations of hot, compressed and highly excited hadronic matter.
- Exotic nuclei far off stability and superheavy elements.
- Nucleus – atomic shell interactions.

Atomic Physics

- Superheavy quasi–atoms and inner shell excitation mechanisms.
- Electron capture and recombination processes.
- Heavy few electron systems.

Theoretical Physics

- Properties of dense hadronic and nuclear matter at finite temperature
- Non-equilibrium transport theory for nuclear collisions

PHELIX Laser Project

- Installation of a Petawatt/Kilojoule Nd:glass laser
- Symbiotic use of intense heavy ion and laser beams
- Generation and investigation of extremely dense and hot matter

Plasma Physics / Beam Physics

- Generation of high energy-density in matter.
- Prestudies for inertial confinement fusion using heavy-ion accelerators.

Materials Research

Biophysics

- Radiation effects in biological systems
- Cancer therapy using heavy ions.

In a near future, a major upgrade of GSI will be performed. The Federal Minister for Educational and Research in Germany has given the project its approval and founding is provided. The plans are to build a new major accelerator ring which will be injected by the current facility, with more than an order of magnitude in rigidity over the present SIS. In addition, more rings to accumulate and store high quality primary and secondary beams, of short–lived exotic nuclei as well as antiprotons, for research in hadronic, nuclear, atomic and plasma physics are also in a far planary stage.

For further information concerning both the present and future GSI, and in some respect also the present status of modern nuclear physics, the highly readable *"Conceptual Design Report"* [86] is strongly recommended.

3.3 Experimental technique and procedure

Prior to the experiment, performed in October 1995, presented here a very similar experiment took place in July 1992. Three PhD theses [87–89] and a handful of articles concerning ^{6,8}He, ^{11}Li and ^{14}Be originate from that early work. The very successful outcome of the pioneering experiment, which increased our knowledge about these dripline nuclei enormously, led to the realization of the second one presented here. This second experiment concerning the same halo nuclei has also proven to be very successful and has so far delivered three more PhD theses [90–92] and many articles, and yet the analysis of the data is still by far not finished. More detailed information can thus be found in the references mentioned above for a reader who has specific interest in some special subject, whether it concerns acceleration techniques, electronics used, data acquisition, detectors, calibration methods etc. which is to vast to be included here.

3.3.1 Beam production

The secondary ^{6,8}He ion beams were produced in fragmentation reactions using a primary stable ^{18}O beam ($\sim 10^{10}$ pps and 340 MeV/u) delivered by the SIS, impinging on an 8 g/cm^2 thick Be–target, see Fig. 3.3.

The requirement for transmission of a certain ion with mass m, velocity v and charge q through a magnetic spectrograph is the equality of the centrifugal and magnetic forces,

$$F = qvB = \frac{mv^2}{\rho} \Rightarrow B\rho = \frac{mv}{q} \approx v\frac{A}{Z} \tag{3.1}$$

where B is the magnetic field and ρ denotes the curvature of the magnet. A selection in vA/Z can thus be done due to the magnetic rigidity, note however that the last approximation only holds for fully stripped ions. Nuclei produced in fragmentation reactions have approximately the same velocity, so in a first approximation v can be regarded as constant.

The 240 MeV/u ^{6}He fragments ($\beta = 0.606$) were separated in the FRS ($B\rho = 7.15$ Tm, $\rho \approx 11.3$ m) and then transported to the experimental area. For isotope selection a wedge-shaped degrader acting as a dispersive element was inserted in the midplane of FRS. The beam intensity was typically 109 ions per spill* and the contaminants were observed on a few percent level only.

*The repetition time was on average 1 pulse per 4.6 s.

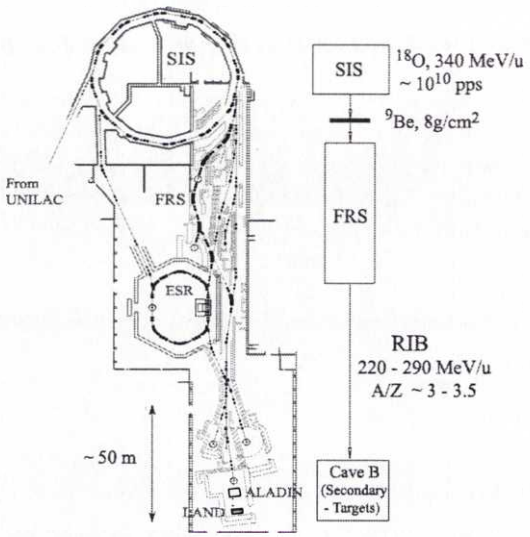

Figure 3.3: *The secondary ^{6,8}He beams were produced by a primary ^{18}O beam preaccelerated in the UNILAC and injected into the SIS for further acceleration to 340 MeV/u. Hereafter the beam underwent fragmentation reactions with an 8 g/cm^2 Be–target creating a full variety of lighter isotopes and transmitted through the FRS where an isotope selection could be made by a $B\rho$ setting. Subsequently the RIB (Radioactive Ion Beam) where transported to the experimental area in Cave B.*

In order to select ^{8}He from other reaction products the transmission through the FRS was achieved with an intrinsic rigidity of 9.21 Tm. Not only ^{8}He was transmitted but also ^{11}Li and ^{14}Be, see Table 3.1. The transmission of these nuclei was facilitated by the extreme relation between neutron and protons these nuclei exhibit, $A/Z \geq 3.5$. Thus as can be seen in Fig. 3.4 only one $B\rho$ selection was necessary for production of these nuclides. A small portion of ^{6}He and tritons was though also transmitted. After transmission through the FRS, the beam was further transported to the experimental area in Cave B.

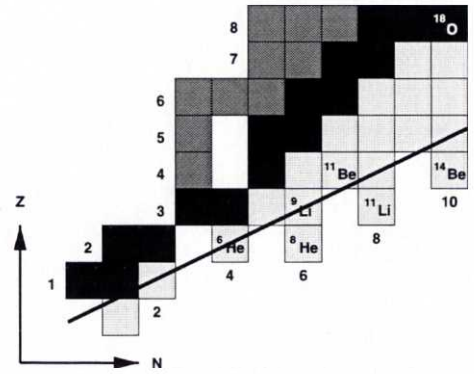

Figure 3.4: *The lowest region of the nuclear chart showing the chosen $B\rho$=9.21 Tm setting in order to transmit the selected nuclides. Only the nuclides below the sloping line are transmitted, if no momentum spread of the secondary ions is assumed.*

Table 3.1: *Velocity and kinetic energy of the ions transmitted at the beam–line setting of $B\rho$ = 9.21 Tm.*

Projectile	^{8}He	^{11}Li	^{14}Be
Kinetic Energy	227 MeV/u	266 MeV/u	289 MeV/u
β	0.593	0.627	0.645
Pulse rate/4.6 s	155	145	30

3.3.2 Complete kinematics experiment set up – Cave B

The experiment was performed in Cave B. The main idea behind the experimental set–up is that charged fragments after breakup in the secondary target, will be influenced by the magnetic field of A LArge–gap DIpole magNet (ALADIN) [93, 94] and deflected from its original path and subsequently detected in a big plastic scintillator, the time–of–flight (TOF) wall. The neutrons created in the break–up process of the secondary beam will, since unaffected by the magnetic field and due to the Lorentzian boost, be focussed into a narrow forward cone around the initial beam direction and directed into the Large Area Neutron Detector (LAND) [95, 96], positioned approximately 11 m downstream from the target. In Fig. 3.5, a schematic view of the experimental set–up in the target area, Cave B is shown.

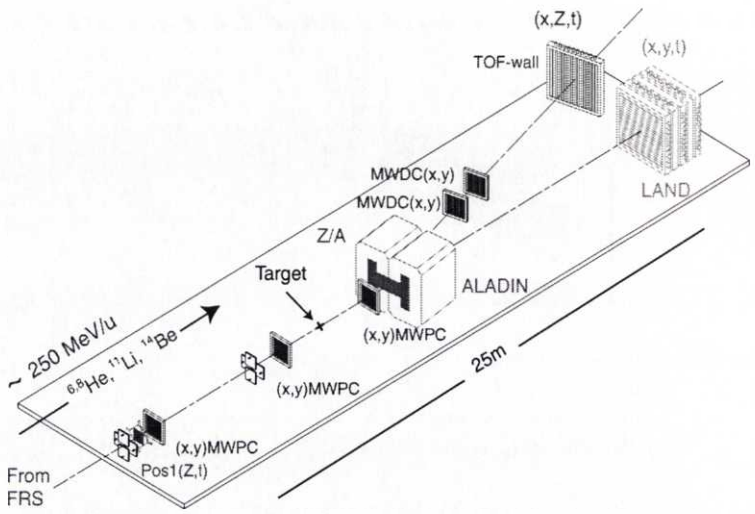

Figure 3.5: *A schematic view of the experimental set–up showing the plastic scintillators Pos1 and TOF–wall, the multi wire proportional chambers (MWPC), the dipole magnet (ALADIN), the multi wire drift chambers (MWDC), and the neutron detector (LAND). The secondary beam particles with energy ~ 250 MeV/u are transmitted from the FRS where the beam direction is from left to right in the figure.*

Beam tracking

The trajectory of the beam before entering ALADIN was determined by three Multi Wire Proportional Chambers (MWPC) [97]. The first two, 9×9 cm^2 in front of the target, and the third one, 20×20 cm^2 located between the target and the magnet served to determine the scattering angle of the fragments. For beam monitoring after the magnet two Multi Wire Drift Chambers (MWDC) 50×70 cm^2 were used, see for example Refs. [87, 88, 90] for a more detailed description of the MWDCs.

A proportional chamber is basically a planar detector consisting of parallel anode and cathode plates with a gas filling in between. If an electric field is applied, the electrons released, in the ionisation process caused by the passage of a charged particle through the gas will drift towards the anode.

If the field is strong enough, an electron will gain sufficient energy to cause secondary ionisation, and a chain of such processes leads to an avalanche of secondary electrons which can be collected as a pulse at the anode. If many anode wires are arranged in a plane between a common pair of cathode plates, each wire acts as an independent detector, and thus the name multiwire proportional chamber.† The position of interaction can be obtained by comparing the signals from different anodes, further the sensitive planes can be arranged in both vertical and horizontal directions giving a two-dimensional image.

MWPCs with high resolution are expensive and might be difficult to handle due to the need of output signals from a very large number of wires. The cost can be reduced significantly and even better spatial resolutions can be obtained in a drift chamber. This uses the fact that released electrons need time to drift from their point of production to the anode. If the drift velocity is known, then the distance from the sensitive wire to the origin of the charged particle can be calculated. Thus, the time delay between the passage of a charged particle through the chamber and the creation of a pulse at the anode, is related to the distance between the particle trajectory and the anode wire. In practice, a reference time has to be defined, for example by the passage of the particle through a scintillator, placed elsewhere in the beam line. Further information concerning drift– and proportional chambers can for example be found in Ref. [99].

A different type of charged particle detectors used in the experiment were scintillator detectors. Here the molecules in the detector material get excited by the incoming particle and subsequently emits light in the deexcitation process. The light output is then converted and magnified in a photomultiplier tube. For time-of-flight measurement a plastic scintillator (POS1) placed in front of the first MWPC was used, together with either a scintillator placed at the end of the FRS or, one of the two MWDCs or the TOF–wall placed behind the last drift chamber at the end of Cave B. The plastic scintillator was also used to determine the charge Z of the incoming ions by means of energy loss in the detector. The charge of the fragments after break–up in the target was subsequently determined by the TOF–wall, composed by 20 scintillator strips arranged parallel to each other along the vertical direction, each with an active volume of $0.5 \times 10 \times 200$ cm^3 covered by a black thin light shield.

†Originally developed by Charpak and collaborators [98], an invention that later rendered him the Nobel Prize in 1992 *"for his invention and development of particle detectors, in particular the multiwire proportional chamber"*, see [66].

Ion identification

In order to select the relevant information for the different reactions, the correct events had to be extracted. First of all it was necessary to distinguish the selected incoming ions (in this case ^{6}He and ^{8}He) from the other fragments in the beam – both before and after the reaction target.

The usual way of ion identification is to plot the mass versus the charge in two–dimensional spectra, or simply the time–of–flight versus the energy loss in a ΔE detector, in this case POS1.

The energy loss by an energetic particle passing through matter stems from the Coulomb interaction with the atomic electrons and can be estimated by using the Bethe–Bloch formula, see e.g. [100].

$$\frac{dE}{dx} = (\frac{e^2}{4\pi\epsilon_0})^2 \frac{4\pi Z_p^2 N_A Z_t \rho_t}{m_e v_p^2 A_t} \Big[\ln(\frac{2m_e v_p^2}{I}) - \ln(1-\beta^2) - \beta^2\Big], \qquad (3.2)$$

where N_A is the Avogadro constant, I the mean ionisation potential of the traversed material, m_e is the electron mass and the subscripts p and t correspond to the projectile and target respectively. The charge Z of the particles can thus be determined from the measured energy loss in the scintillator detectors using the above relation.

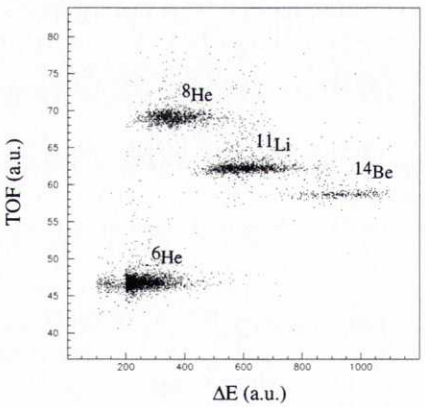

Figure 3.6: *Identification of the incoming ions could be made in TOF versus ΔE–plots. The incoming ^{6}He, ^{8}He, ^{11}Li and and ^{14}Be are well separated.*

As can be seen in Fig. 3.6 a very clean separation could be obtained using this method, yielding reliable identification of the incoming ions by imposing two–dimensional cuts in the spectra. A similar identification was performed after the breakup in the target.

Neutron detection – LAND

Neutron detection in general presents a significant experimental challenge as neutrons do not have electric charge. This fact makes the interaction with matter an improbable process since the atomic electrons, making up the size of the atom, can be completely disregarded. Instead the neutrons interact with the nuclei only through the short range strong interaction, which means that a neutron detector must detect the secondary charged particles from a strong interaction process. Furthermore there is no reliable way of getting the total energy of the neutron by studying the energy deposit inside a detector as the energy varies strongly with scattering angle. Thus, time–of–flight methods must normally be used for this purpose.

The LAND detector (see Fig. 3.7) consists of 200 paddles each $2\times0.1\times0.1$ m^3 arranged 20 by 20 in 10 successive layers, alternating vertically and horizontally aligned. Each paddle has an altering sandwich structure of 5 mm scintillator/5 mm passive iron converter in order to increase the detection efficiency. The incoming neutrons interact with the iron nuclei by producing hadronic showers that are detected in the scintillator material. The light produced by secondary charged particles is collected by light guides on both ends of the scintillator sheets and directed to the photomultipliers. The difference in arrival time of the two signals serves to localize the position of the neutron incidence and the arrival time is deduced from the mean timing of the two signals. An internal calibration of LAND with regard to time and position is obtained by tracing cosmic rays through the detector between the beam spills. The detection efficiency for 240 MeV neutrons in LAND is quite high, 85 ± 5 %, and more thorough explanation of the detector properties can be found in Ref. [95].

In front of LAND, a veto detector for charged particles is installed, consisting of 20 thin organic scintillator strips to discriminate the neutrons from charged particles not deflected enough by ALADIN. The strips are arranged parallel to each other along the horizontal direction. Each strip covers an area of 200×10 cm^2, which matches the paddle size in LAND, and has a thickness of 0.5 cm which is sufficient for charged particles to interact within it, but to thin for a noticeable neutron interaction.

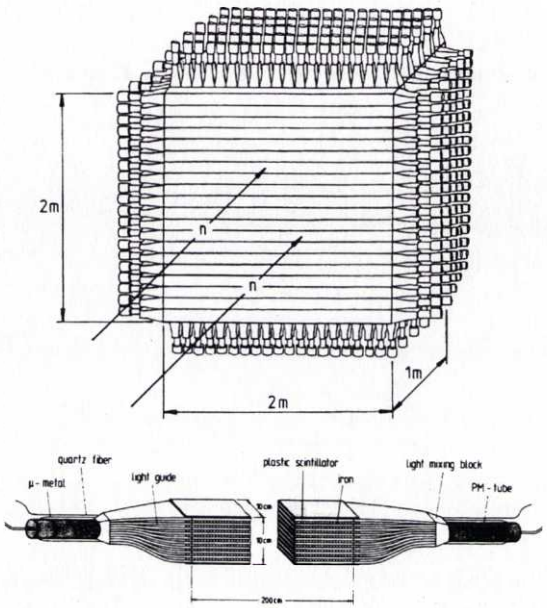

Figure 3.7: *A schematic view of the Large Neutron Area Detector (LAND), the lower inset shows the construction of one its 200 paddles. (From Ref. [95].)*

Neutron disentanglement

All events were classified according to the apparent neutron multiplicity m_n = 0,1,2 registered in LAND, and thus m_n characterizes the reaction mechanism. For each neutron multiplicity, integrated cross sections were determined, taking into account corrections for the detection efficiency and limited acceptance.

One of the problems analyzing the data is a background connected to the finite multiple–hit resolving power of the detector [101–103]. Neutrons impinging onto LAND fire a number of its submodules and a pattern algorithm has to be employed in order to disentangle multiple neutron hits. The algorithm and its performance, under the circumstances of an experiment very similar to the present one is described in Ref. [102]. The main effect appears as a reduced double–hit recognition capability in the case when two neutrons interact in a close vicinity of each other in LAND. Such detection

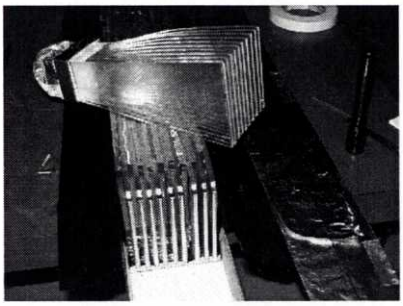

Figure 3.8: *A photograph showing a disassembled paddle of LAND. The altering sandwich structure of the plastic scintillator and iron converter is clearly seen.*

deficiencies were corrected for using realistic event simulations adjusted to the present experiment, and utilizing the LAND response from calibration measurements with tagged neutrons. A correction for reactions taking place outside the target, for example in a detector, was accomplished by the measurement without a target.

Data acquisition and analysis tools

One of the main tools for on– and off–line analysis was the acquisition and control software, PAW–LAND, based on the PAW (Physics Analysis Workstation)/ZEBRA [104] software package, developed at CERN and extended for experiments in Cave B [105, 106]. The experimental data on–line were written as LMD (List Mode Data) files event–by–event and hereafter converted into N-tuples for off–line analysis.

CHAPTER 4

Observables and extracted information

Due to the short life time of nuclei in the vicinities of driplines, much experimental information about their structure is obtained through their collision with stable targets. In this chapter different tools, some of them used in the present analysis, for probing the nuclear structure are briefly reviewed and in addition a few theoretical approaches are mentioned.

First, to extract information about observables such as relative energy, angular distributions etc., the momenta of the particles involved are needed. In the experiment performed here, the longitudinal momentum in the laboratory system, p_z, could be determined directly by time–of–flight measurement through

$$p_z = m_0 \gamma \beta, \tag{4.1}$$

where $\beta = v/c$, $\gamma = (1/(1-\beta^2))^{1/2}$, m_0 is the rest mass of the fragment and v is expressed in units of c. The transverse momenta, $p_{x,y}$, could then be calculated using

$$p_{x,y} = p_z \cdot \theta_{x,y}, \tag{4.2}$$

where $\theta_{x,y}$ expressed in radians, is the angular deflection of the fragment perpendicular to the beam direction measured after the breakup target. The momenta of the neutrons were calculated in a similar way, and the wanted information could subsequently be transformed into the appropriate reference frame and coordinate system.

4.1 Break-up reactions and cross sections

The most important reaction mechanisms in the intermediate and high energy range with halo- and other loosely bound nuclei are Coulomb and nuclear dissociation. The dependence of the cross section on the target for these processes vary approximately as Z^2 and $A^{1/3}$ respectively. For light targets, the Coulomb effects are small, and nuclear contribution dominates and since the charge dependence grows much faster than that of the mass number, electromagnetic processes play the most important role for high Z targets. It should however be noted that the cross section cannot be unambiguously subdivided into nuclear and Coulomb parts.

In the experiment described here, carbon and lead targets were used. In addition runs without a target, so called *empty target* runs, needed for background subtraction and calibrations were also made. The cross section for a specific reaction could thus be calculated by using

$$\sigma = \frac{M}{\omega N_A}\left[\frac{N_{sr}^{t}}{N_{ip}^{t}} - \frac{N_{sr}^{et}}{N_{ip}^{et}}\right], \tag{4.3}$$

where the different variables denotes,

M : the molar mass of the target in g/mol

ω : the target density in g/cm^2

N_A : the Avogadro constant

$N_{sr}^{t(et)}$: the measured number of events for a *s*pecific *r*eaction, with target (t) or empty target (et), e.g. ^{8}He $\rightarrow$ ^{6}He + 2n

$N_{ip}^{t(et)}$: the measured number of *i*ncoming *p*rojectiles that can give this reaction e.g. ^{8}He, with target (t) or without target (et).

One of the major differences between exotic neutron- or proton rich halo nuclei and tightly bound nuclei is the larger probability for the former to break up owing to the smaller binding energy of the halo cluster.

Fig. 4.1 illustrates the possible break-up reactions for halo nuclei. The different processes are often referred to as halo nucleon stripping (4.1.1:c,d), core stripping (4.1.1:e,f), diffractive dissociation (4.1.1:a) and Coulomb dissociation (4.1.1:b). From a theoretical point of view, stripping denotes the

removal of one or several halo constituents regardless what happens to the removed nucleons. However, from the experimental point of view the reactions are often described in terms of detectable signatures. The term absorption means removal of the core or/and halo nucleon(s) in a way that they cannot be detected, while the signal of core break-up is detection of the halo nucleons in coincidence with fragments from the shattered core.

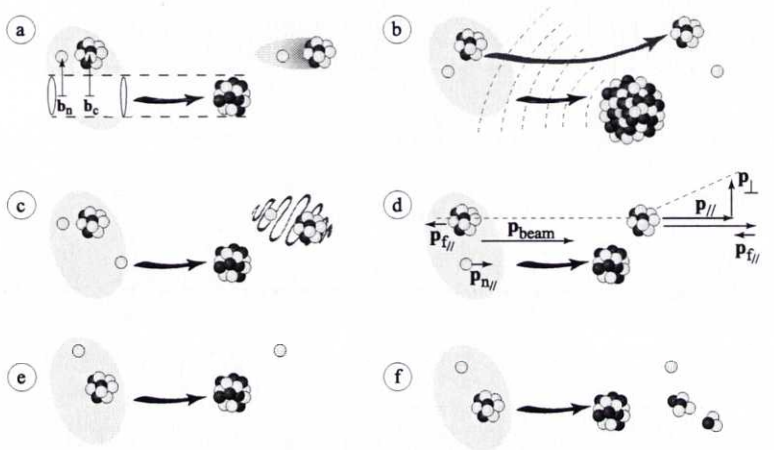

Figure 4.1: *Schematic illustration of different break-up channels and concepts for halo nuclei. Part a) illustrates diffractive break-up where all constituents escape the target creating a cylindrical cut in the wavefunction. Also shown is the impact parameter* **b** *which defines the distance between the center of mass of the target and that of the projectile. Part b) shows Coulomb break-up that also leaves all clusters to be detected. Parts c) and d) exemplify halo nucleon absorption. In part c) The FSI (final state interaction) is indicated, and in part d) the principle of measuring the internal $p_{\parallel}$ and $p_{\perp}$ is sketched. Parts, e) and f) show the core stripping processes of core absorption and core break-up, respectively. (Courtesy K. Markenroth.)*

Theoretical investigations of reactions with loosely bound nuclear systems started as early as 1947 with work done by Serber [107]. Here the interaction between the removed nucleon and the target is neglected, i.e. the target is assumed to be totally transparent. Today nuclear reactions at intermediate and high energies are often treated in the eikonal approximation [108], valid if the energy is high and the scattering angle is small [109]. See also

Ref. [110] where the eikonal model was used for studying nuclear breakup of Borromean nuclei. The form known as Glauber theory has been widely used for calculating reactions at high energies. The method was originally developed by Glauber [111], assuming that the target nucleus could be viewed as an absorbing black disc. Due to diffraction when a part of the wave function of the projectile is removed, the projectile no longer remains in its ground state but instead contains an admixture of excited states. When these excited states are unbound the probability of dissociation becomes a fact. For recent investigations using Glauber theory, applied to halo interactions with light targets, see e.g. the papers by Bertsch, Brown and Sagawa [112, 113] and Parfenova et al. [114, 115].

Theoretical methods treating break-up reactions without building on the eikonal approximation are of course also existing. One of them is Distorted Wave Born Approximation (DWBA) calculations, where the basic idea is to excite the system above the cluster threshold and then break it apart, see e.g Ref. [116], and also [117] for recent development applied to ^{6}He. Methods which include coupling to the continuum are the transfer-to-continuum model [118], and the Continuum Discretized Coupled Channels (CDCC) method [119].

4.1.1 Decoupling core and halo

The decoupling of core and halo degrees of freedom is manifested in the important relation between the interaction cross section and the halo removal cross section derived by Ogawa, Yabana and Suzuki [120]

$$\sigma_{-halo}(A) = \sigma_I(A) - \sigma_I(A - halo). \tag{4.4}$$

This formula is based on Glauber theory with the assumption that the total wavefunction of the system factorizes into a core- and a halo part. Furthermore if there are more than one nucleon in the halo no bound subsystem should exist (Note however the recent paper by Zheng et al. [16], studying the two-neutron halo structure of ^{16}C). This relation offers an opportunity to experimentally test the clusterization in a specific nucleus. The experimental neutron removal cross sections and total interaction cross sections for the one-neutron halo ^{11}Be, and the two-neutron halos ^{6}He, ^{11}Li and ^{14}Be do all satisfy the relation (4.4) reasonably well for high energy fragmentation in carbon targets [20]. The same relation tells us that ^{6}He is not a good core inside ^{8}He, see e.g. Paper II.

4.1.2 Coulomb dissociation

In applying Coulomb excitation to studies of unstable nuclei, it is practical to provide the unstable nuclei as a beam. Hence the projectile is to be excited by the Coulomb field of a high Z-target. When the impact parameter is larger than the range of the strong interaction, reactions between a projectile and target can only proceed via the long range electromagnetic interaction. For a weakly bound halo nucleus the result of this interaction is, with high probability, dissociation, while in the case of a "normal" nucleus, excitation of either the projectile and/or the target occurs. Due to this, halo structures have an extremely large Coulomb dissociation cross section (predicted in [12] and confirmed for the first time in [121]), even up to 80 times larger than expected from the Z^2 dependence, comparing the interaction cross sections of ^{11}Li [102] and ^{12}C [122] with a lead target.

Figure 4.2: *Photograph of Jupiter and the comet Shoemaker-Levy 9 taken by the Hubble Telescope on May 18, 1994. The gravitational interaction of Jupiter with the comet broke it up in many pieces, seen as a string in the bottom part of the figure. (From European Space Agency Information Centre [123].)*

The situation is similar to what happened with the comet Shoemaker-Levy in 1994 which crashed on the surface of Jupiter. Approximately 2 hours after closest approach, the comet (which was presumably a single body at the time) was broken apart by tidal forces into at least 21 pieces [123], clearly seen in Fig. 4.2. The pieces continued to orbit Jupiter two years before impacting on the planet due to the gravitational forces when Jupiter approached the Sun.

Coulomb excitation is a well established experimental probe in nuclear physics [124, 125]. The measured Coulomb-excitation cross section is a direct function of the electromagnetic matrix elements $\mathrm{B}(E\lambda)$ and $\mathrm{B}(M\lambda)$, and can be deduced through the theory of Coulomb excitation [124].

For halo nuclei, the experimental cross sections for Coulomb dissociation are large enough to provide a good opportunity to measure all halo particles after the reaction. Small momentum transfer or large impact parameters determine the reaction implying that all halo particles are most likely, only marginally disturbed in the process.

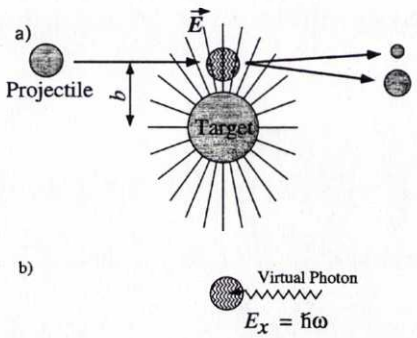

Figure 4.3: *(a) A schematic drawing of the Coulomb excitation process. The projectile is exposed to the electric field, $\vec{E}$, from the target in the projectile rest frame, and thus Lorentz–contracted in the beam direction. The final state is depicted as as a fully dissociated state. (b) The electric field from the target is interpreted as a virtual photon flux. (From T. Nakamura PhD Thesis [126].)*

The E1 strength distribution $dB_{E1}(E)/dE$ can be deduced from the Coulomb dissociation cross section by using the equivalent photon method* , see for example Refs. [126, 129, 130] and references therein. Here the collision effect between a relativistic charged particle and a target is replaced by the corresponding effect produced by the interaction of radiation. Hence, the Coulomb excitation can be expressed as a photo-absorption process induced by a virtual photon, as schematically depicted in Fig. 4.3.

*The method is also referred to as Weizäcker-Williams method of virtual quanta [127, 128].

The theory of Coulomb dissociation for high energy beam projectiles on a heavy target is well known [131] and the calculated differential cross section for $E1$ transition, $d\sigma/dE$ can be obtained by multiplying the E1 strength function $dB_{E1}(E)/dE$ with the virtual photon spectrum $N_{E1}(E)$ which is given in [131]

$$\frac{d\sigma}{dE} \sim N_{E1}(E)\frac{dB_{E1}(E)}{dE}. \tag{4.5}$$

4.2 B(E1) strength and sum rules

The extremely weak binding energy of halo nuclei gives rise to strong effects associated with coupling to the continuum. It is therefore essential to study both resonant and non-resonant continuum transitions, and decompose the multipole strength.

The analogy between ^{11}Li and the deuteron was stretched even further by Hansen and Jonson [12] (referring to among others, Oppenheimer, Mullin and Guth [132, 133]), speculating that such a loosely bound nucleus as ^{11}Li would have a soft electric dipole mode which could easily be excited in Coulomb collisions.

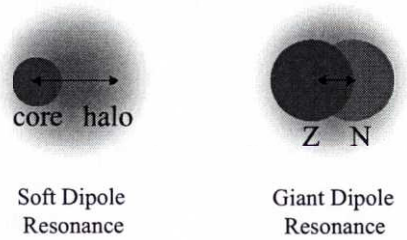

Figure 4.4: *Schematic illustration of Soft Dipole Resonance and Giant Dipole Resonance*

The electric dipole (E1) strength in stable nuclei is largely exhausted by a giant dipole resonance, constructed from a superposition of many particle-hole excitations with essentially no E1 strength appearing in the low energy region below 5 MeV. This is, however, not the case for some light halo nuclei. It has been suggested that the giant dipole resonance could split into two components. One component would correspond to the normal frequency, i.e. an oscillation of the core protons against the core neutrons (ΔT = 1 isospin

change) and the other to a low frequency i.e. an oscillation of the core against the halo neutron(s) (ΔT=0), illustrated in Fig. 4.4. The latter has been referred to as a soft dipole mode.

In general, this 'soft dipole strength' i.e. the strength well below the giant dipole resonance, is expected for neutron rich nuclei with loosely bound valence neutrons. The transition between the first excited $I^\pi = 1/2^-$ state at $E^* = 0.32$ MeV and the $I^\pi = 1/2^+$ ground state in ^{11}Be representing one of the strongest E1 transitions ever observed (B(E1)=0.1 e^2fm^2) between particle bound levels [134]. Such a favored E1 transition may be induced by a decoupled feature of the valence neutron and an extended single particle wave function of the loosely bound neutron. The measurement of the low-lying E1 strength has been extended to the continuum excitation of many loosely bound neutron rich nuclei ^{11}Li [102, 135–137], ^{11}Be [138], ^{14}Be [139], ^{19}C [140] among others, where the halo neutrons play an essential role to increase the strength. In ^{11}Be, the E1 transition between the ground state and the ^{10}Be+n continuum has been observed to be even one order of magnitude larger than that between its bound states [138].

Furthermore, the E1 sum rules (see e.g. [109]), which characterize the strength of the transition can be used to estimate the size, and in some respect the deformation, of a system. The sum rules thus provide a direct link between the experimentally measured transition probabilities and the geometry of the ground state. And by using the Non Energy Weighted cluster sum rule [109],

$$B(E1) = S_{dus}^{NEW} = \frac{3}{4\pi} Z_c^2 e^2 \langle \Delta r_c^2 \rangle, \tag{4.6}$$

information of the ground state structure can be gained. Δr_c here describes the distance between the c.m. of the core and the whole nucleus, see e.g. [141] and Paper II.

4.3 Momentum distributions

An important issue in the interpretation of experiments with loosely bound nuclei have been the shapes and widths of the momentum distributions. These two properties are closely related as pointed out in [13, 142], see also [43, 143, 144] and references therein.

Measurements of fragment momentum distributions after fragmentation have for several decades been an important tool in investigating the internal

velocity distributions in stable nuclei. The extraction of the momentum distribution is usually complicated by a number of effects; the divergence of the beam, the angular straggling in the target and the beam monitoring detectors and reactions not originating from the target. The divergence and the angular straggling can be handled by studying the distribution from the non–reacting ions, and the background can be subtracted with help from runs without a target. However, the method is rather well understood which is a necessity for experimental investigations close to the unexplored driplines. Projectile fragmentation at high energy ($\geq$ 400 MeV/u) has e.g. shown the following characteristics of stable nuclei [145, 146]:

(i) The momentum distribution in the fragment frame of reference is Gaussian.

(ii) The shape for the core part is the same in the beam direction, $p_{\parallel}$, and the direction perpendicular to the beam, $p_{\perp}$.

The width of the momentum distribution, $\sigma(p_{\parallel})$, is found to be more or less independent of the beam energy and the target mass, but dependent on the projectile and fragment mass numbers, A_P and, A_F respectively. This dependence can be expressed as

$$\sigma(p_{\parallel}) = \sigma_0 \sqrt{\frac{A_F(A_P - A_F)}{(A_P - 1)}} \tag{4.7}$$

where $\sigma_0 = 90$ MeV/c, first formulated by Goldhaber and Heckman [145].

The relatively high cross sections for the breakup of halo nuclei and the possibility of a relatively simple interpretation have led to the examination of fragment momentum distributions not only as a signature of a halo distribution, but also as a probe of the nuclear structure. This due to the possibility to obtain wave functions in the momentum space which can be transformed by using Fourier transformation into spatial coordinates.

After the pioneering experiments of Kobayashi et al. [147], measuring the momentum distributions of charged fragments from breakup of ^{6}He, ^{8}He and ^{11}Li, the technique has been one of the main tools used to explore the halo feature, where the distribution has been found to be more narrow than in stable nuclei. The narrow distribution may be qualitatively seen as a direct consequence of the Heisenberg uncertainty principle which states that an object with large spatial extension has a narrow width in phase space;

$\Delta x \cdot \Delta p \geq \hbar/2$. It can be noted that the pronounced halo nuclei core distribution have Lorentzian shapes, see e.g [43].

It has further been shown that $p_\perp$ is more sensitive than $p_\parallel$ to Coulomb and nuclear diffraction, requiring a good reaction theory [148]. In addition, it has also been shown that not only the reaction cross section but also the transverse momentum distribution of the fragments are sensitive to the separation energy of the last neutrons and to the size of the density profile in these nuclei [147]. These two quantities are linked since the size of the nucleus is roughly proportional to the inverse of the square root of the separation energy. Using the Goldhaber model for soft fragmentation, Tanihata and collaborators [147] were able to relate the narrow peaks in the transverse momentum distributions with the separation energies and sizes of the radioactive nuclei.

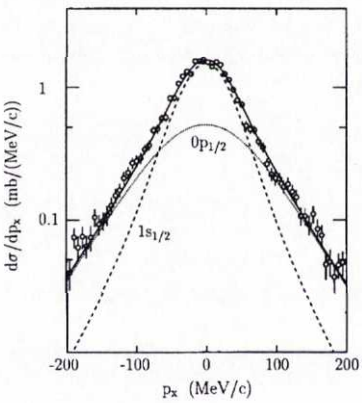

Figure 4.5: *Transverse momentum distribution of ^{10}Li reconstructed from the momenta of ^{9}Li + n in the reaction of ^{11}Li on a carbon target. The decomposition of the distribution into angular momentum components $l = 0, 1$ is shown. The solid line represents a fit with a 45% $(1s_{1/2})^2$ contribution. (From H. Simon et al. [149].)*

A recent and very successful experiment measuring the transverse momentum distribution of ^{10}Li from the one neutron knock–out of ^{11}Li is presented in [90, 149]. Here it was shown that the shape seen in Fig. 4.5 only could be fitted with a superposition of $s^2 + p^2$ components with about 50% abundance of each.

As a remark, it should however be noted that, in a single halo-nucleon knockout reaction the momentum distribution of the remaining fragment

does not resemble the complete internal momentum distribution of the removed nucleon. The higher momentum components of the halo wave function, which are located mainly inside the core, cannot be determined in halo-breakup reactions by measuring the final channel only because at small impact parameters the core will be destroyed in the reaction. Core shadowing has to be included in the extraction of the halo wave function from the momentum distribution of the residual fragments [150, 151].

4.4 Invariant mass

In particle physics the invariant mass method is a widely used tool searching for resonance states, and during the last years the method has proven to be very successful in nuclear physics as well.

The characteristic interaction time for a strong decay process is approximately the time for a fast particle ($v \approx c$) to traverse a nucleus i.e. $10^{-15} \times 10^{-8} = 10^{-23}$ s. Fast decays like this are impossible to *see*, and can only be observed as peaks in distributions from scattering processes and therefore called resonance particles or just resonances.

In order to determine the mass and lifetime of such a resonance, the intensity or cross section is usually plotted against the invariant mass, M_{inv}, of the decay products, defined by:

$$M_{inv}^2 c^4 = \left(\sum_{i=1}^{n} E_i\right)^2 - \left(\sum_{i=1}^{n} \vec{p}_i\right)^2 c^2, \tag{4.8}$$

where the left hand side of the equation is invariant and has the same value no matter what reference frame is used, and the right hand side denotes the energies (E_i) and momenta ($\vec{p}_i$) of the decay products. This is the natural definition since it is consistent with the usual relation between energy and momentum of a relativistic particle ($E^2 = \mathbf{p}^2c^2 + m^2c^4$) after use of energy-momentum conservations.

One of the first resonance particles discovered this way was the ρ^0 meson [152], which can be formed in pion–nucleon collisions and decays rapidly to π^+ and π^- through

$$\pi^- + p \rightarrow \rho^0 + n$$

$$\rho^0 \rightarrow \pi^+ + \pi^-.$$

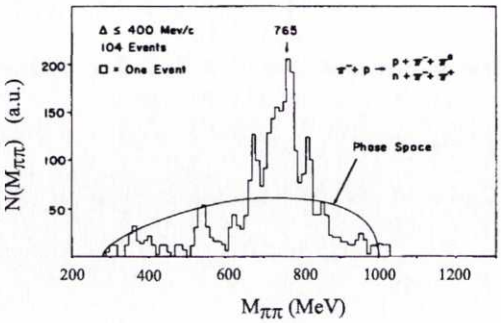

Figure 4.6: *The invariant mass spectrum for the $\pi^-\pi^+$ system in the $p(\pi^-, \pi^+\pi^-)n$ reaction. The ρ^0 resonance at 765 MeV is clearly seen. (After A. R. Erwin et al. [152].)*

However, the reaction could also occur without the intermediate ρ^0–state

$$\pi^- + p \rightarrow \pi^+ + \pi^- + n.$$

Thus in both cases the particles actually observed are the two pions. Therefore, as can be seen in Fig. 4.6, the invariant mass distribution has two components, a continuous background (a phase space – stemming from the two pions, with a minimum at $2m_\pi c^2$ to a maximum determined by the incident beam energy) and a peak at a definite energy, 765 MeV, corresponding to the mass of the ρ^0 meson.

The energy of a decaying state is not sharp and the probability distribution has a Lorentzian shape, usually called a Breit–Wigner distribution [153] (The formalism was originally developed by Breit and Wigner for describing resonances while studying the absorption by thermal neutrons [154]). The lifetime τ, of each resonance is directly related to the resonance width Γ, at half maximum, through

$$\Gamma = \frac{\hbar}{\tau}. \tag{4.9}$$

Particle physics experiments are usually performed with very high beam energy, leading to strongly forward focused particles, thus facilitating a coincident detection of all involved particles. In this way the invariant mass of the selected product can be extracted. However, in nuclear physics experiments, beams of low energy have traditionally been used making it im-

possible to detect all particles in coincidence due to large scattering angles. These experiments have been limited to the missing mass method of the type *A(B,fragment+n)X*, a method which is still commonly used today at low and intermediate energies. If X is detected the missing mass provides the energy of the *fragment+n* system, where peaks can be associated to resonances. Obviously it is experimentally more complicated to detect all fragments, including neutrons, than just one fragment. The big advantage detecting all fragments is however quite obvious that the *wanted* system is the *detected* system, and in addition, that correlations between the different fragments can be accessed.

With the development of high energy beams and larger detector setups, coincident detection of all fragments have become possible also in nuclear physics experiments. During the last ten to fifteen years the invariant mass method has been successfully used in nuclear structure studies at the dripline, see e.g. [155]. However, here the search is not for new particles but for different resonance states in the nuclei.

In the projectile system, the energies of all detected particles are small and nonrelativistic expressions can be used to calculate the relative energy in the *fragment + Xn* system. The resulting relative energy spectrum differs from the invariant mass spectrum only in the energy scale by the subtracted masses of the involved fragments.

If a reaction proceeds via a resonance, the energy spectrum can be explained using the R–matrix formalism [156] using a Breit–Wigner parameterization of the resonance

$$\frac{\mathrm{d}\sigma}{\mathrm{d}E} \propto \frac{\Gamma(E)}{(E - E_r)^2 + (\frac{1}{2}\Gamma(E))^2}, \tag{4.10}$$

where E_r is the resonance energy [157].

A very good example of the usefulness of the method can be found in [141], seen in Fig. 4.7, where the relative energy of ^{6}He was reconstructed from the measured momenta of the two neutrons and the α–particle after break up in a carbon target. As can be seen in the figure a resonance at an excitation energy of 1.8 MeV is clearly distinguished from the rest of the spectrum.

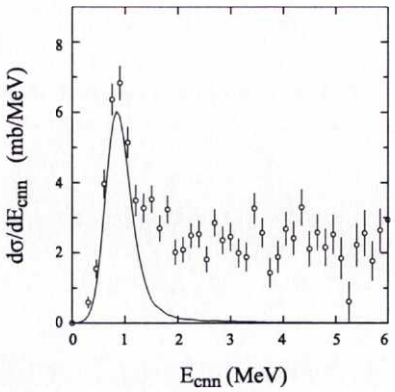

Figure 4.7: *Relative energy spectrum reconstructed from the measured momenta of the two neutrons and the α-particle after dissociation of 240 MeV/u ^{6}He in a carbon target. The energy E_{cnn} denotes the energy above the two-neutron separation threshold, S_{2n} = 0.973 MeV. Data points are shown as open circles with error bars. The solid line represents a Monte-Carlo simulation assuming a 2^+ state in ^{6}He at an excitation energy of 1.797 MeV (Γ=0.113 MeV). (After T. Aumann et al. [141] and Paper I.)*

4.5 Energy and angular correlations

At the high beam energies accessible at GSI the velocities of the halo nuclei ($\beta \approx 0.6 - 0.7$) are much larger than the Fermi velocity of the corresponding halo nucleons ($\beta < 0.1$). The internal degree of freedom of the halo nuclei may therefore be considered to be "frozen" during the collision process, thus reflecting a "snapshot" of the halo in momentum space.

In analogy to $\gamma-\gamma$ angular correlation studies [158], the angular momenta of the participants in the sequential decay can be determined through the emitted neutrons [159]. The fragmentation processes of Borromean nuclei are dominated by a two-step mechanism, where in the first stage, one neutron is knocked out while the rest of the system remains untouched [38, 160]. The residual unbound two-body system subsequently decays into a neutron and a charged fragment. This two-step process leads to angular correlations relative to the propagation direction of the unstable fragment, governed by the quantum numbers of the intermediate state.

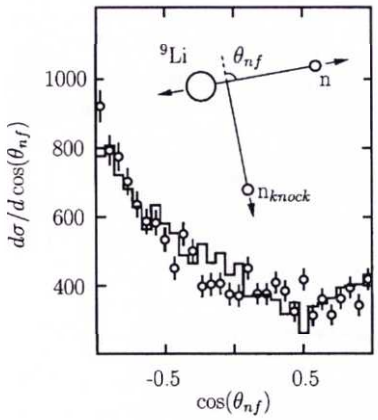

Figure 4.8: *Angular distributions from the decay of ^{10}Li. The points are experimental data and the histogram is a reconstruction corrected for resolution and acceptance effects. Note the strong forward–backward asymmetry, which reflects the $l = 0, 1$ interference. (From H. Simon et al. [149].)*

The inset in Fig. 4.8 defines the correlation angle θ_{fn} between the recoil direction of the A - 1 system after one neutron knockout, and the relative motion between the charged fragment and the remaining neutron in the reaction. The technique where the relative phase (see e.g. [161]) between the components of the wave function can be determined proved to be very successful when applied to ^{11}Li, observing the angular distribution of the decay products from the recoiling ^{10}Li in the one neutron stripping reaction in a carbon target [90, 149]. In Fig. 4.8 the strong forward–backward asymmetry demonstrates the interference of the $l = 0, 1$ final states in the single–neutron removal. The theory of the angular distribution has e.g. been discussed by Garrido et al. [162] who successfully predicted the asymmetry in ^{11}Li.

The correlations in two-particle decay can easily be extended to the three-particle decay case that is commonly encountered in particle physics experiments and typically analyzed using the technique developed by Dalitz [163]. The technique has also been successfully used in nuclear physics experiments, see e.g. the recent paper by Fynbo et al. [164] analyzing the three-body decay of the 12.71 MeV state in ^{12}C.

Another powerful approach to reveal correlation effects between fragments is the mixed-event method. This method is frequently used while analyzing elementary particle physics experiments to estimate a background from particles which may be decay products of resonances (see e.g. [165–167]). The method has also been used successfully for the search of two particle reso-

nances in fragmentation reactions [157, 168]. It can also be used to eliminate background contributions[†] by generating uncorrelated events. This along with the technique of intensity interferometry has been worked out by Zajc et al. [171] and Marqués et al. [172], see also the pioneering work on stellar interferometry by Hanbury-Brown and Twiss [173] and the review of intensity interferometry by Boal, Gelbke and Jennings [174].

[†]Background is here understood as a peak like structure in the relative energy spectrum not stemming from a real resonance, see e.g. [169, 170].

CHAPTER 5

Results and discussion

The main idea of this chapter will be both to summarize, and to some extent go further into detail of what is presented in Papers I–V.

First, we focus on the intermediate unbound nucleus ^{7}He stemming from the one-neutron knock-out of ^{8}He. Second, we concentrate on ^{8}He itself and its breakup reactions in two different targets, carbon (1.3 g/cm^2) and lead (0.387 g/cm^2). Hereafter the results for the unbound neutron rich hydrogen isotopes ^{4}H and ^{5}H originating from the one-proton knock-out of ^{6}He on a carbon target (1.87 g/cm^2) will be presented in detail. After each element (helium and hydrogen) a small section will be devoted to a short discussion and summary of the analysis performed.

5.1 Papers I and III : The unbound ^{7}He

The ^{7}He ground state is fairly well known and is situated about 440 keV above the (^{6}He+n) threshold [34]. In different experiments [175–177] an excited state at about 3.3 MeV above this threshold has been observed. In paper I the discrepancy between the experimental data at low relative energy, and a single resonance description was accepted as a first evidence for an unknown excited state in ^{7}He. A detailed analysis presented in Paper III confirmed the existence of a new state in ^{7}He, at 1.0 MeV above the ^{6}He+n threshold, not observed before.

Events with one neutron detected in coincidence with a ^{6}He fragment formed after fragmentation reactions of the ^{8}He beam in a carbon target were selected in this analysis. Detection of only one neutron implies that the second one either has been absorbed or deflected strongly after a large momentum transfer. Such a reaction corresponds to a one-neutron knock-out or a one-neutron stripping [38]. The reaction mechanism can be considered as a sudden neutron removal, due to the very high beam energy ($\beta \approx 0.6$), where the rest of the system remains almost unperturbed.

The ground state of ^{7}He is a comparatively long lived resonance ($\Gamma \approx 160$ keV, which corresponds to a lifetime of approximately 1200 fm/c) and thus decays far away from the reaction zone. This provides the basis for a model with a two step mechanism in the sudden approximation: (1) Knock–out of a neutron from ^{8}He into the unstable ^{7}He nucleus. (2) Subsequent decay of ^{7}He into ^{6}He and a neutron. The sudden approximation neglects momentum transfer to the ^{7}He subsystem in the knock–out reaction, giving a resulting momentum of ^{7}He equal to the momentum of the neutron knocked out from the projectile but in opposite direction [178], schematically illustrated in Fig 5.1. The momentum distribution of the fragment spectator ^{7}He is thus determined by the internal momentum distribution of the removed neutron, which in turn is determined by the projectile ground state wave function.

The momentum distributions extracted from the data will not be discussed here, but is presented in Paper I and compared with theoretical models.

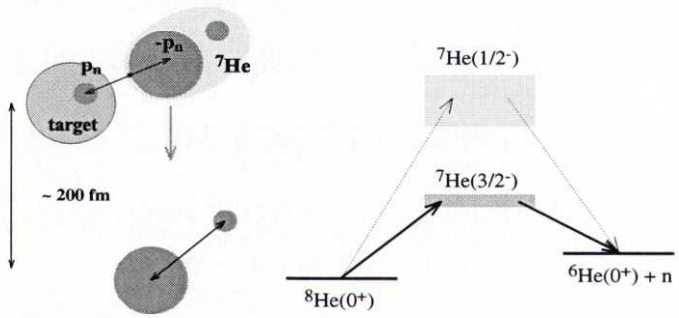

Figure 5.1: *Illustration of the one neutron knock–out as a two step mechanism. The beam direction is from top to bottom in the left figure.*

In Paper I, the angular distribution of decay neutrons from ^{7}He was found to have a correlation function

$$W(\theta) \sim 1 + 0.7(1)\cos^2(\theta) \tag{5.1}$$

where θ is the angle between the ^{7}He momentum vector and the decay neutron. The decrease of the anisotropy term as compared to ^{5}He [38] may be attributed to a more complicated structure of ^{8}He (compared to ^{6}He), which most likely has a component of an excited ^{6}He in its ground-state configuration, together with a strong admixture of a $(p_{1/2})^2$ component.

5.1.1 Relative energy — A new state

The relative energy distribution E_r between the ^{6}He fragment and the neutron, was reconstructed from the measured momenta of the neutron, $\mathbf{p}_n$ and ^{6}He, $\mathbf{p}_{^6He}$, with

$$E_r = \frac{m_{^6He} + m_n}{2m_{^6He}m_n}\mathbf{p_r^2} \tag{5.2}$$

and is shown in Fig. 5.2 as open circles with error bars*.

The experimental data was first compared with an expected resonance energy distribution for the population of the ^{7}He ground state with the resonance parameters adopted from Ref. [34] (resonance energy $E_r = 0.44$ MeV and width $\Gamma = 0.16$ MeV, shown as a solid line in Fig. 1, Paper III). The calculation was performed using the Monte-Carlo method with a Breit-Wigner shaped resonance, following the procedure outlined in Ref. [157], and including effects of the experimental resolution and acceptance. As can be seen, the experimental data cannot be described assuming a population of the ^{7}He ground state alone. The calculated curve describes the maximum of the cross section well but decreases too fast towards higher energies compared to the experimental data.

In order to describe the whole spectrum it was necessary to include one additional resonance. The attempt to describe the experimental spectrum in a free parameter fit with one single resonance resulted in the minimal reduced χ^2_{red} equal to about 2.8. However, the best fit using two resonances, shown as the full drawn line in Fig. 5.2, was achieved with $\chi^2_{red} = 1.5$, with the position of the ground state at $E_r = 0.43(2)$ MeV ($\Gamma = 0.15(8)$ MeV) and the second state at $E_r = 1.0(1)$ MeV ($\Gamma = 0.75(8)$ MeV). We interpret the second resonance, with a fraction of $35 \pm 10\%$ of the total cross section for

*$\mathbf{p}_r = m_{^6He}m_n/(m_{^6He} + m_n)\,(\mathbf{p}_{^6He}/m_{^6He} - \mathbf{p}_n/m_n)$.

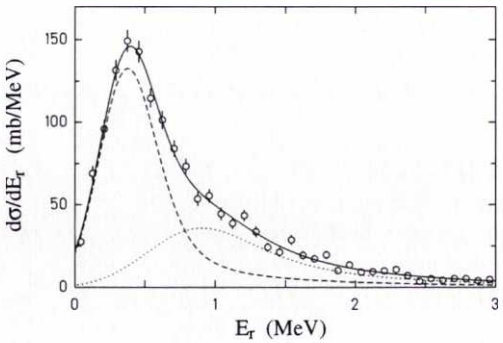

Figure 5.2: *Coincidence cross section of the ^{6}He-n system after breakup of 227 MeV/u ^{8}He on a carbon target as a function of relative energy E_r. The lines show the decomposition of a fit to the data (solid curve) into the ground state (dashed curve) and the proposed first excited state (dotted curve), using an R-Matrix expression folded with the experimental acceptance and response. From Paper III, Fig. 2.*

the one-neutron knock-out channel, as the $I^\pi = 1/2^-$ state of ^{7}He. Fig. 5.3 shows the dependence of χ^2 on the resonance parameters Γ_1 and Γ_2 if two resonances are assumed, and a clear minimum in χ^2 can be distinguished for the parameters given above. Similar, and consistent with the one shown here, contour plots are shown in Fig. 3, Paper III, illustrating the parameter dependence on the positions of the two resonances.

In this context it is also important to note that the same experimental setup and the same data analysis procedure was used for the ^{5}He data, where the α–n cross section is dominated by the $p_{3/2}$ ground state [157]†. It should also be mentioned that the lifetime of the excited state is as well comparatively long, approximately 200 fm/c, and thus leads to a decay far away from the reaction zone.

In three earlier experiments [175–177] a state has been found at an energy of about 3.3 MeV above the ^{6}He+n threshold. This state was first interpreted as corresponding to a neutron in the $p_{1/2}$-orbital and ^{6}He in the ground state. However, the data presented in Ref. [175] showed that this resonance mainly decays into the 3n+α channel, which implies that the most probable configuration is of the form $[^6\mathrm{He}^*(2^+) \otimes 0p_{1/2}]_{5/2^-}$.

†Note also, a very recent experiment performed at GANIL [179], where the data shows indication of an excited state in the energy region found here.

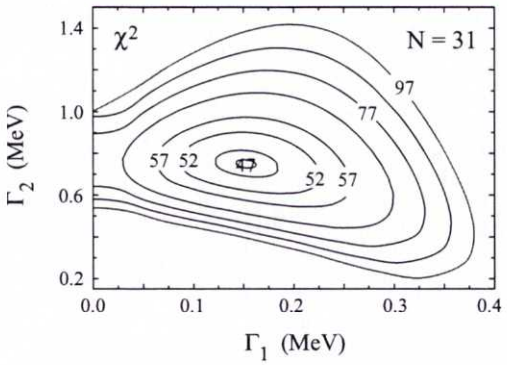

Figure 5.3: *Contour plot showing the dependence of χ^2 for the N=31 degrees of freedom on the resonance parameters Γ_1 and Γ_2 if two resonances are assumed. For each point on the contour lines all remaining parameters were varied in order to minimize χ^2 again.*

With this interpretation one would expect the position of the ^{7}He($1/2^-$) resonance, with a neutron in a $p_{1/2}$-state coupled to the ^{6}He(g.s.), 1.8 MeV lower in energy. With the selection of the ^{6}He+n channel, made in the present experiment, the $5/2^-$ state is excluded from the data set indicating that the state we observe at 1.0 MeV has another origin. With all these evidences the most reasonable I^π assignment to the state observed here is $1/2^-$. Further evidence for the spin-parity assignment $I^\pi = 1/2^-$ comes from recent calculations of the ^{7}He system where the sequence of negative-parity states $3/2^-$(g.s), $1/2^-$, $5/2^-$ has been obtained [22, 180–182].

The smaller anisotropy term in ^{7}He, extracted from the angular distribution, may also be seen as an evidence for the I^π=$1/2^-$ assignment to the state at 1.0 MeV. This, since a mixing of the $p_{3/2}$ ground state with the $p_{1/2}$ channel would cause a diminishing of the anisotropy, which is actually what we see. The contribution from the $1/2^-$ state was estimated to be only 7% in ^{5}He [38] compared to 35 ± 10% in ^{7}He.

In addition, the proximity of the two spin-orbit partners in ^{7}He would also give an important clue for the understanding of the ground state structure in ^{8}He. The relative contribution from the $1/2^-$ state indicates a strong admixture of a $(0p_{1/2})^2$ component in the ^{8}He ground-state wave function, discussed thoroughly in Paper I.

5.2 Papers I and II : ^{8}He — A complicated structure

In this analysis, mainly the break up channels of ^{8}He into ^{6}He + 2n were investigated. Due to limited acceptance, the α + 4n cannel was outside the range of the present setup. In Papers I and II comparisons with the ^{6}He break up into α + 2n were made, however we will here concentrate on the heavier of the two unstable He isotopes.

Table 5.1: *Experimentally determined excited states in ^{8}He. Excitation energies E^* above the ground state and resonance widths Γ are given in MeV.*

Ref.	E^*	Γ	E^*	Γ	E^*	Γ
[183]			2.8(4)			
[184]	1.3		2.6(3)	1.0(5)	4.0(3)	0.5(3)
[185]			3.57(12)	0.50(35)		
[49]			3.59(6)	0.5	4.54(15)	0.70(25)
[177]					4.4(2)	1.8(2)

The present experimental knowledge about excited states below 5 MeV in ^{8}He is summarized in Table 5.1. In addition, the recent experiment by Iwata et al. [186] should be noted. Here the ^{8}He dissociation into ^{6}He + 2n on a Sn target shows a peak in the relative energy spectrum at E^* = 3.6 MeV, Γ = 0.5 MeV. This was interpreted as the first excited 2^+ state, however no fit to the data was performed.

From these data one might conclude that ^{8}He has two resonances below 5 MeV, one in the energy interval from 2.6 MeV to 3.6 MeV and the other between 4.0 MeV and 4.6 MeV. The low energy resonance has been interpreted as the first excited 2^+ state, which is supported by the measured differential cross section for inelastic scattering on a hydrogen target [187]. The nature of the resonance around 4 MeV is not known.

5.2.1 Carbon target — Two resonances

By using different targets, different reaction mechanisms can be studied. In the first experiment a carbon target was used, and due to a low Z–value one would mainly expect nuclear interaction to be dominant in the reaction mechanisms.

Cross Sections

In Paper I, a detailed discussion concerning different reaction channels in the break up of ^{8}He into fragment and neutrons, and further what kind of information that could be extracted from this, is presented.

This discussion will not be repeated here, but the main conclusions were:

- The interaction cross section for ^{8}He together with the measured neutron removal channels give evidence for breakup into α+4n, interpreted as a signature of the five-body character of ^{8}He.
- The cross section for the one-neutron knock-out channel shows evidence for configurations with neutrons in the $0p_{1/2}$ shell as well as a core excited configuration, ^{6}He*+2n, in the ^{8}He ground state.

Relative Energy

The relative energy spectrum as determined from the measured momenta of ^{6}He and neutrons after inelastic excitation of 227 MeV/u ^{8}He is shown in Fig. 5.4. The experimental distribution may, in principle, be treated as one single broad resonance. However, the statistical evidence of a narrow structure at low energy and the existing experimental information on ^{8}He levels which was discussed above, indicate that the most plausible explanation is the presence of two overlapping resonances. This interpretation is also supported by the following two observations:

- The width of the observed structure is at least twice as large as expected for any p-states from single-particle limit [188] and it can therefore hardly be due to one single 2^+ state.
- The cross section is about 30 mb (the same as for excitation of ^{6}He in the entire interval from 0 up to 10 MeV, see [141] and Paper I) which seems to be too large for the excitation of one single 2^+ state.

The solid line in the figure corresponds to a Monte-Carlo calculation using two Breit-Wigner shaped resonances. The fit to the spectrum resulted in the position of the first resonance at 2.9 ± 0.2 MeV ($\Gamma = 0.3 \pm 0.3$ MeV) and the second resonance at 4.15 ± 0.20 MeV ($\Gamma = 1.6 \pm 0.2$ MeV). Note, that the parameters of the high energy resonance are in good agreement with those obtained in the stopped-pion-absorption experiment [177] and the resonance at 2.9 MeV is in good agreement with the results given in Refs. [183, 184].

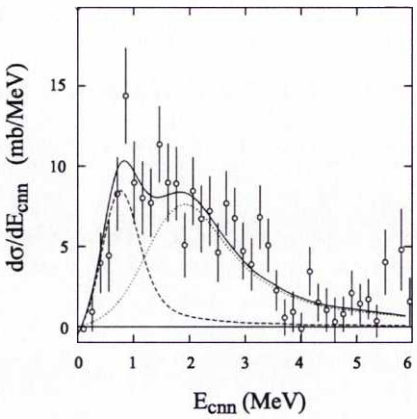

Figure 5.4: *Relative energy spectrum reconstructed from the measured momenta of the two neutrons and ^{6}He after dissociation of 227 MeV/u ^{8}He in a carbon target. E_{cnn} denotes the energy above the two-neutron separation threshold (S_{2n} = 2.14 MeV). Data points are shown as open circles with error bars. The solid line represents a Monte-Carlo simulation assuming a 2^+ resonance at an excitation energy of* 2.9 ± 0.2 *MeV* ($\Gamma = 0.3 \pm 0.3$ *MeV) and a resonance at* 4.15 ± 0.20 *MeV* ($\Gamma = 1.6 \pm 0.2$ *MeV). The dashed and the dotted lines display separate contributions of the two resonances. From Paper I, Fig. 5.*

If the lowest excited state corresponds to a neutron in $p_{1/2}$-shell and a hole in $p_{3/2}$-shell one would expect two states, 2^+ and 1^+, close to each other. This expectation comes from recent theoretical predictions using large-basis shell-model calculations which place the 2^+-state at $E^* \approx 5$ MeV [22], and from quantum Monte-Carlo calculations [180] which result in $E^* = 2.3$ MeV. The second excited state is in both calculations a 1^+ state at an energy about 2.5–3 MeV above the 2^+ state. The characteristics of the known lowest excited states of the neighboring $N = 6$ nucleus ^{10}Be (two 2^+ states at 3.37 and 5.96 MeV and a 1^- state at 5.96 MeV) confirm the 2^+ assignment of the low energy resonance but indicate that the second resonance might be either a second 2^+-state or a 1^- state, or an overlap of both. The measured angular distribution of the excited ^{8}He may shed light on the momentum transferred in the reaction and, hence, on the quantum numbers of the unknown 4.15 MeV state.

Angular Distributions

Quite generally, through a study of the angular distribution of the decay products, it is possible to determine the spin of the parent nucleus.

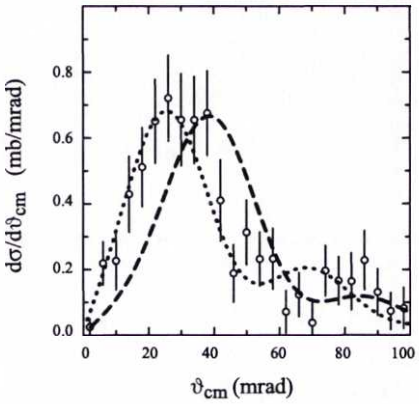

Figure 5.5: *Differential cross sections for inelastic scattering in a carbon target of 227 MeV/u ^{8}He as a function of the center-of-mass angle. The experimental data are compared to calculations in a distorted-wave Born approximation (DWBA). The dotted line corresponds to a nuclear dipole transition (λ=1), and the dashed curve represents a calculated quadrupole transition (λ=2). All theoretical distributions are corrected for the experimental resolution in the experiment. From Paper I, Fig. 6.*

The sum of momenta ($\mathbf{p}_{n_1} + \mathbf{p}_{n_2} + \mathbf{p}_{^6He}$) represents the total momentum ($\mathbf{p}_{^8He}$) of the ^{8}He system. The differential cross section as a function of the angle between the direction of the incoming beam and the center of mass of the outgoing system in the projectile-target c.m. system, ϑ_{cm}, is shown in Fig. 5.5.

The broad ^{8}He state at 4.15 MeV in the relative excitation energy spectrum contributes with about 80% to the cross section in the inelastic scattering channel and thus determines the main features of the experimental angular distribution. Does the cross section obtained for excitation of the narrow state at 2.9 MeV in ^{8}He suggest a quadrupole transition as in the ^{6}He (see Refs. [141, 189] and Paper I) case? Since the two states strongly overlap and the contribution from the narrow state is small, the differential cross section for excitation of this state cannot be obtained directly.

Following the procedure outlined in Paper I, DWBA calculations (see also Ref. [190]) for nuclear dipole and quadrupole transitions were made. The result of the calculation for the quadrupole transition is shown in Fig. 5.5 as a dashed line and the predicted peak position is close to the experimental one in the spectra, however, the experimental data clearly shows a shift of the peak towards smaller angles. The experimental distribution agrees better with a calculation assuming a $\lambda = 1$ excitation shown by the dotted line in the figure. Note, that we did not use any free parameter to adjust the position of the peak. This observation leads to the conclusion, that, in contrast to the fragmentation of ^{6}He, where a quadrupole transition dominates, the dipole mode is the strongest one in the excitation of ^{8}He. A conclusion which became even more obvious while analyzing the interaction with the heavier lead target.

5.2.2 Lead target — Strong interference

In the second experiment lead was used as a target. With a much higher Z–value than the carbon target one would here expect Coulomb interaction to be the dominant reaction mechanism.

The statistics for this experiment were not as good as with the lighter target, but good enough to make a careful analysis and extract qualitative information from the data.

Cross Sections

The different cross sections from corresponding reaction mechanism (see Table I, Paper II) and how they were extracted is described in detail in Paper II, and the main conclusions were:

- The one-neutron knock-out channel, dominating the fragmentation in a light target, is still an important part of the fragmentation in a lead target. The electromagnetic contribution to this channel is negligible.

- The Coulomb dissociation cross section for reactions in a lead target was evaluated from the experimental data by three different methods. It was found that the cross section for the ^{8}He dissociation is a factor 3 smaller than that for ^{6}He.

Angular Distributions

The broad resonance observed at $E^* = 4.15$ MeV in the ^{6}He+2n relative energy spectrum with the carbon target (see Fig. 5.4) was tentatively assigned to have $I^\pi = 1^-$. Since Coulomb excitation from the ground state would result in a final state with exactly this spin-parity, one would expect interference between Coulomb and nuclear dipole transition amplitudes to this state.

To check this, the nuclear and Coulomb amplitudes were calculated using the DWBA approach [190], described in detail in Paper II. The result is shown as a dashed and dotted line in Fig. 5.6 for the nuclear and Coulomb part respectively. As can be seen none of the transitions describe the data very well and the amplitudes were therefore added coherently: $\frac{d\sigma}{d\Omega} = \frac{k_f}{k_i}|f_C(\theta) + f_N(\theta)e^{i\phi}|^2$. The best fit to the data was obtained with $\phi = \frac{\pi}{2}$, which can be seen as a solid line in the figure.

The result is quite striking, since neither Coulomb (as in the ^{6}He case, see Refs. [141, 189] and Paper II) nor nuclear excitations separately can describe the experimental data. Contrary to the case of ^{6}He, where the Coulomb interaction plays a dominant role, the ^{8}He inelastic scattering is governed by both nuclear and Coulomb interactions. Moreover, the interference results in a shift of the oscillations towards the positions of the experimental distribution, which also can be seen as an evidence for the Coulomb-nuclear interference. These calculations also show that one cannot unambiguously subdivide the inelastic cross section into nuclear and Coulomb parts. We may thus conclude that the observation of Coulomb-nuclear interference provides further support for the $I^\pi = 1^-$ assignment.

Further, the B(E1) strength for ^{8}He was calculated from the estimated EM inelastic cross section in the angular distribution, to a value of 0.38 ± 0.07 e^{2}fm^2 assuming a Breit–Wigner shaped distribution using the adopted energy for the 1^- state. This value is approximately a factor three to four smaller than that of ^{6}He.

In addition, by using the Non Energy Weighted cluster sum rule, Eq. 4.6, a comparison between the deformations Δr_c (describing the distance between the c.m. of the core and the whole nucleus) can be made, as explained in Paper II. The conclusions from these estimates is shortly summarized as: ^{8}He is characterized by a more uniform distribution of the four neutrons around the α–particle core, than are the two neutrons in ^{6}He around the α-core.

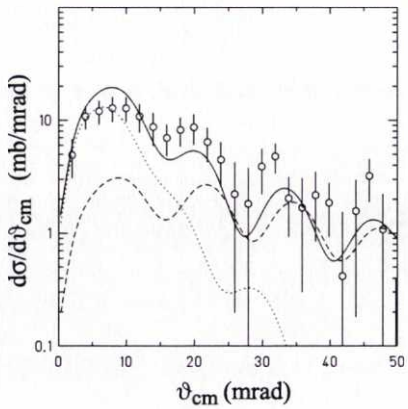

Figure 5.6: *Differential cross sections for inelastic scattering of 227 MeV/u ^{8}He in a lead target as a function of the center-of-mass scattering angle. The experimental data are compared to calculations in distorted-wave Born approximation (DWBA). The dotted line displays the DWBA calculations for electric dipole λ=1 Coulomb excitation, while the dashed line shows the results of DWBA calculations with nuclear dipole λ=1 excitation, and the solid line corresponds to a superposition of the two excitation modes. All calculations are corrected for the experimental resolution. From Paper II, Fig. 1.*

5.3 Discussion Papers I – III

The results obtained from the present analysis have hopefully shed some new light on the structure of heavy helium isotopes. Note however, that all the cross sections analyzed here correspond to data with ^{6}He in the exit channel.

The comparison between the data for ^{6}He and ^{8}He as presented in Papers I and II has shown that the structure of the latter is very complex and supports its description as a five-body system. To complicate the situation even further, our findings show that a core excited configuration, ^{6}He*+2n exists in the ^{8}He ground state, which also quite recently has been observed in Refs. [58, 191]. Further again worth mention, is the observation of a 1^{-} resonance in ^{8}He easily excited by nuclear interaction. This would resemble the similar phenomena found e.g. in ^{11}Li, interpreted as associated with a soft dipole mode, where the valence neutrons oscillate against the core. In this context, the similarity with ^{6}He is again quite striking remembering the

large width of a possible low lying 1^- state above a 2^+ state [34].

However, to fully uncover the nature of this intricate system more precise data are required. In particular, a detection system capable of registering all the fragments in the five-body channel (α + 4n) needs to be implemented.

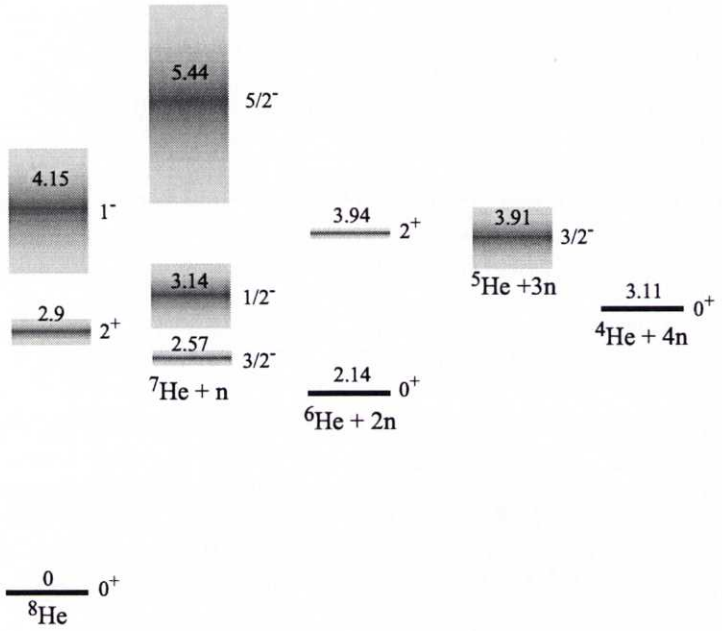

Figure 5.7: *Proposed level scheme of the heavy helium isotopes. Note that all spin and parity assignments correspond to the respective He isotope. The parameters of the two excited states in ^{8}He and the ground and first excited state in ^{7}He are taken from the work presented here (energies in MeV).*

The proposed level scheme of the heavy helium isotopes based on the work presented here is shown in Fig. 5.7. (Note that ^{5}He is taken to be unbound with 0.80 MeV in this scheme, using data from Ref. [34], whereas the same state presented in Fig. 4, Paper III is unbound with 0.89 MeV, using data from Ref. [192].)

The energy difference between the ground state and the excited state in ^{7}He obtained here is about 0.6 MeV, which should be compared to the lowest estimate of this energy difference in ^{5}He which is 1.2 MeV [34, 193, 194].

We thus find a considerable decrease of the splitting of the two lowest states when adding two more neutrons to ^{5}He[‡]. We note that the spin-orbit force is proportional to $-(1/r)dV/dr$ so that systems with large spatial extension tend to show a smaller splitting. The difference in size and diffuseness between ^{4}He and ^{6}He should therefore be reflected in the current observation.

5.4 Paper IV : ^{4}H — A test case

The data presented in Paper IV and V was obtained in proton knock-out reactions from a 240 MeV/u ^{6}He beam on a carbon target. Nucleon knockout is the dominant reaction mechanism at this energy, and Glauber type models are well suited to describe the data. The ^{6}He structure is predominantly an inert α-core with two valence neutrons in the $p_{3/2}$-shell with their momenta coupled to zero [195]. A sudden knockout of a proton from the α-particle would result in a system with a triton and two valence neutrons in the same configuration as in the projectile.

The process is thus similar to that discussed in Ref. [196] describing an experiment where the one-proton and the one-neutron knock-out reaction from ^{11}Be and ^{11}Li respectively was used to investigate the properties of ^{10}Li. We may further assume that the one-proton removal transforming helium to hydrogen, proceeds via a direct reaction due to the large difference in the neutron– and proton separation energy of ^{6}He, which makes proton evaporation very unlikely.

We will here first focus on ^{4}H, constructed from events containing only one neutron detected in coincidence with a charged triton from the one-proton knockout channel of ^{6}He. This data was mainly used as a check of the assumed reaction mechanism by comparing with previously published data from the extensively studied ^{4}H [33].

The overall experimental resolution with regard to the decay energies for the studied reaction channels was obtained from Monte-Carlo simulations, calculated applying the measured detector responses. The general trend in both the two-body (t+n) and three-body (t+n+n) system is the same, where at low decay energy the resolution is about 150 keV and increases to 800 keV at 8 MeV, see Fig. 5.8. The Monte-Carlo simulations also give the detection efficiency. In the two-neutron case at low energy a decrease in efficiency due

[‡]Note also that the splitting between the $3/2^-$ ground state and the first excited $1/2^-$ state in the bound isotones ^{7}Li and ^{7}Be are 0.478 and 0.429 MeV, respectively [34].

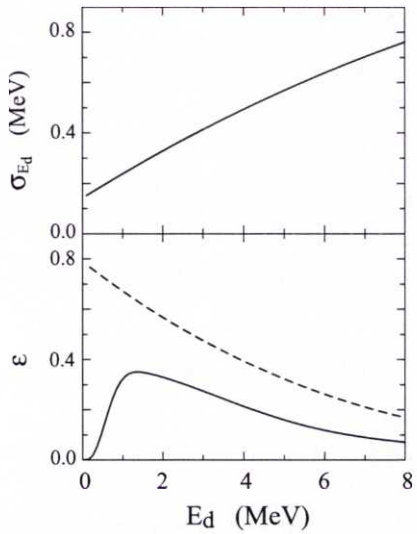

Figure 5.8: *Top: Overall resolution σ_{E_d} with regard to the decay energy E_d for ^4H into one neutron and a triton, and ^5H into two neutrons and a triton. The curve was obtained from Monte-Carlo simulation, calculated applying the measured detector responses. Bottom: The two lines show the efficiency for the experimental set up, where the dashed and solid line corresponds to ^4H and ^5H respectively.*

to the limited resolving power for two neutrons at small relative distances in LAND is observed. Further, due to the finite solid angle of the neutron detector the efficiency also decreases at higher energies. All the measured distributions were corrected for efficiency which includes distortions introduced by the tracking routine and restricted acceptance of the experimental setup.

As can be seen in Fig. 5.9 the I^π=2$^-$ ground state of ^{4}H is overlapping with the 1$^-$ first excited state, both are about 3 MeV broad and predicted to be separated by only 300 keV. The states have the same structure, i.e. a neutron in the $p_{3/2}$ shell coupled to the triton core. Since in ^{6}He, the two neutrons are predominantly occupying the $p_{3/2}$ shell [15], the sudden one-proton knockout from ^{6}He as studied here is expected to populate both the 2$^-$ and 1$^-$ states in ^{4}H. However, since both states are much broader than their separation in excitation energy ($\sim$ 300 keV), and as can be seen

in Fig. 5.8 we are not able to resolve the two resonances at the energy of interest, only one peak is expected in the $\frac{d\sigma}{dE_{tn}}$ experimental spectrum. The higher lying 0^- and 1^- states arising from a neutron in the $p_{1/2}$ shell coupled to the triton will only be weakly populated due to the small weight of the $(p_{1/2})^2$ configuration in the ground state of ^{6}He.

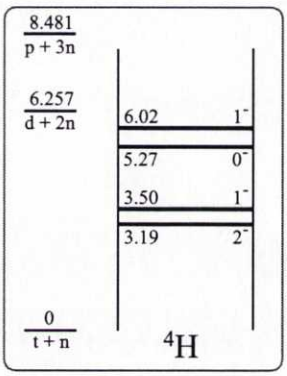

Figure 5.9: *Schematic illustration of the energy levels in ^4H (energies in MeV), the data is taken from [33].*

The data was analyzed using the invariant mass method constructing a relative energy spectrum in the t+n center of mass system (E_{tn}), shown in Fig. 1, Paper IV. The experimental distribution, can be fitted almost perfectly by using a single Breit-Wigner shaped resonance, with E_λ=3.56(9) MeV, E_R=2.67(9) MeV and Γ^{obs}=3.28(12) MeV. Here E_λ is the formal resonance position, E_R is the real resonance position and Γ^{obs} is the observed width, see e.g. Ref. [156] for details.

The extracted parameters are in agreement with experiments where ^{4}H was studied in different nuclear reactions by the missing mass method (see compilation [33]). However, one notes that the maximum in the measured relative energy spectrum (Fig. 1, Paper IV) is at about 1.6 MeV of the t-n relative energy, while the experimental excitation function for n-t elastic scattering is peaked at 2.6 MeV [197], shown as data points in Fig. 5.10.

In order to understand this effect, the elastic scattering cross section was calculated using the R-matrix expression [156]

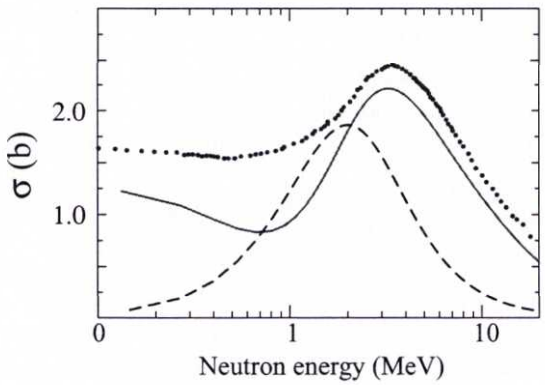

Figure 5.10: *Experimental excitation function for $n-t$ elastic scattering from Ref. [197], shown as data points. The solid line represents the elastic scattering cross section calculated with the R-matrix expression in Eq. 5.3 using the resonance parameters obtained in the fit to the ^4H relative energy spectrum presented here. The dashed line shows the cross section (scaled with a factor 0.5) calculated using only the resonance term in Eq. 5.3, see text.*

$$\sigma = \frac{\pi}{k^2}\Big[4(2l+1)\sin^2\varphi_l - g_J\Gamma_\lambda\frac{2(E_\lambda+\Delta_\lambda-E)\sin 2\varphi_l + \Gamma_\lambda(1-\cos 2\varphi_l)}{(E_\lambda+\Delta_\lambda-E)^2+\frac{1}{4}\Gamma_\lambda^2} + g_J\frac{\Gamma_\lambda^2}{(E_\lambda+\Delta_\lambda-E)^2+\frac{1}{4}\Gamma_\lambda^2}\Big], \tag{5.3}$$

where φ is the hard sphere phase, k the wave number and g_J the statistical spin factor. Using the resonance parameters obtained in the present work, with $l = 1$ and $R = 4$ fm and without any additional parameters, the peak position of the experimental excitation function for n-t elastic scattering from Ref [197] could be reproduced, shown as a solid line in Fig. 5.10. For more details see Ref. [156] and also Paper IV.

The last term in Eq. 5.3 is the so called resonance term, the second is the interference term and the first is the potential scattering term. The reason for the shift of the maximum is interference between potential and resonance

scattering, and thus the position of the maximum in the experimental distribution is dependent on the reaction mechanism. The effect is most pronounced in connection with broad resonances and might be the reason for the scatter of the experimental data on the resonance position. In some cases, the ^{4}H resonance position was only determined from the maximum in the measured spectrum [33]. A similar case concerning ^{5}He and ^{5}Li is discussed in [198].

5.5 Papers IV and V : ^{5}H — The t+n+n system

Encouraged by the consistency of the ^{4}H data and that we now understand the reaction mechanism well, we turn to the ^{5}H case where two neutrons are registered in coincidence with a triton after the one-proton knockout reaction from ^{6}He.

The experimental studies of ^{5}H began four decades ago with an evidence that it is β-unstable with a half-life of about hundred ms [199]. Since then, the quest for ^{5}H has been undertaken in many laboratories, and today the consensus is that a stable ^{5}H does not exist.

Several attempts to find the resonance in different types of nuclear reactions have been unsuccessful. Evidence for ^{5}H as a broad state at 5.2(4) MeV was obtained in the ^{7}Li(^{6}Li,^{8}B) reaction [200]. A recent experiment reports the ground state at 5(1) MeV with a width of 3 MeV in ^{9}Be(π^-,pt) and ^{9}Be(π^-,dd) reactions [54]. However, a peak in a spectrum of protons from the ^{3}H(t,p) reaction, consistent with a ^{5}H state at 1.8 MeV, was found in Ref. [201]. The observation of the ^{5}H ground state at 1.7(3) MeV with the width 1.9(4) in the ^{6}He(p,2p) reaction was reported [56] about a year ago. The most recent experiment, again using the ^{3}H(t,p) reaction revealed a peak in the experimental spectra of protons consistent with a ^{5}H resonance at the same energy as in Ref. [56] but with a width less than 500 keV [55, 202].

5.5.1 Relative energy — A broad structure

The distribution of the total kinetic energy in the three body system E_{tnn}, which is an equivalent of the invariant mass spectrum, was obtained from the measured momenta of the neutrons and the triton and is shown in Fig. 5.11 as data points. The observed structure exhibits a width of about 6 MeV (FWHM) with a maximum at about 3 MeV.

A conventional analysis using a Breit-Wigner formula, as was carried out for the ^{4}H case, is not appropriate to analyze broad few-body systems, and

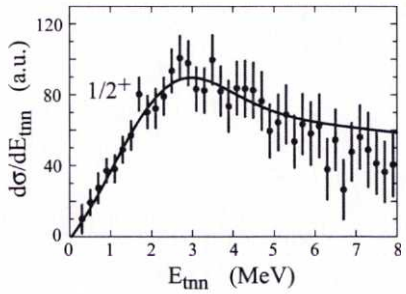

Figure 5.11: *The relative energy spectrum of the t+n+n-system obtained in one-proton knockout reactions with a ^{6}He beam at 240 MeV/u impinging on a carbon target. The experimental data are shown by circles with statistical uncertainties. The solid line is the result of a three-body microscopic calculation for the t+n+n system, assuming $I^\pi = 1/2^+$ [52]. From Paper IV, Fig. 3 and Paper V, Fig. 1.*

the maximum of the spectrum, at about 3 MeV cannot be accepted as the resonance position without theoretical analysis.

The spectrum was therefore compared with calculations made within a strict three-body t+n+n dynamics [52], with $I^\pi = 1/2^+$, E_{tnn} = 2.5-3.0 MeV and Γ = 3-4 MeV. As can be seen in Fig. 5.11, good agreement is achieved between the experimental data and the shape of the calculated distribution with $I^\pi = 1/2^+$, considered to be the ground-state configuration in ^{5}H [52]. Note, that the reason for the relatively narrow width as compared with the calculated decay through the di-neutron channel (discussed in Chapt. 2), is due to the three-body nature of the state. However, to independently confirm the $I^\pi = 1/2^+$ assignment, an analysis of the energy and angular correlations in the t+n+n system was performed.

5.5.2 Energy and angular correlations — Similarities with ^{6}He

Two different approaches were used to reveal correlation effects between the different fragments in the t+n+n relative energy spectrum.

First, the influence of the t-n and n-n final state interactions on the relative energy spectrum was analyzed using an event-mixing procedure. Second, in order to obtain the relative weights of the predominant partial waves and to assign the spin and parity of the broad structure seen in the t+n+n relative energy spectrum, the experimental energy and angular correlations were

evaluated using a restricted set of hyperspherical harmonics (HH), see Appendix A.

The procedure using the mixed event method is in detail discussed in Paper IV. This analysis showed that di-neutron decay is dominating at low relative energy, counteracting a narrow ^{5}H resonance, while the sequential neutron emission determines the spectrum at higher energies, see Fig. 4, Paper IV. Therefore both n-n and t-n correlations are of vital importance for the ^{5}H resonance.

To obtain more qualitative estimates, the energy and angular correlations were hereafter analyzed using a more refined approach, aiming at determining the spin and parity characterizing the system.

The three body configuration can be expressed by the angle (ϑ) between the Jacobi momenta, by the total energy of the three-body system and by the energy shared by corresponding pair of particles, see Appenidix A. Two different Jacobi sets were used, **A** and **B**, see Fig. 2, Paper IV. The variable $\varepsilon_{tn} = E_{tn}/E_{tnn}$ in Jacobi set **A** or variable $\varepsilon_{nn} = E_{nn}/E_{tnn}$ in Jacobi set **B** determines the ratio of relative energy for each pair of particles, where evidently $0 \leq \varepsilon \leq 1$.

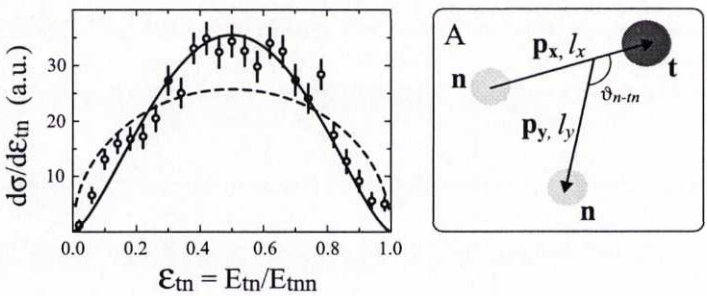

Figure 5.12: *Left: Energy correlation shown in Jacobi configuration* **A** *$(n-tn)$. The experimental data are shown as open circles with statistical uncertainties. The dashed line corresponds to a conventional phase space distribution, while the solid line shows a distribution with relative angular momenta $l_x = l_y = 1$. Right: Illustration of Jacobi momentum coordinate system* **A**.

The energy distribution shown to the left in Fig. 5.12 looks at first glance similar to that expected from a conventional phase space distribution

$$d\sigma/d\varepsilon \sim \sqrt{\varepsilon(1-\varepsilon)}. \tag{5.4}$$

However, this phase space distribution shown as a dashed curve cannot reproduce the experimental data.

For a three-body system, where no narrow resonances exist in any of the binary subsystems, the following equation holds [203]

$$d\sigma/d\varepsilon \sim \varepsilon^{l_x+\frac{1}{2}}\,(1-\varepsilon)^{l_y+\frac{1}{2}} \tag{5.5}$$

where l_x and l_y are the angular momenta in the t-n and n-tn subsystems, respectively. The experimental distribution shown in Fig. 5.12 can be reasonably well approximated by equation (5.5) with $l_x = l_y = 1$, shown as solid line, indicating that the main contribution to the final state wave function mainly stems from p-shell configurations. Thus, having roughly determined the main components of the angular momenta for the two neutrons in the final state wavefunction we proceeded one step further, analyzing the angular and energy correlations using the method of HH expansion proposed in Ref. [204].

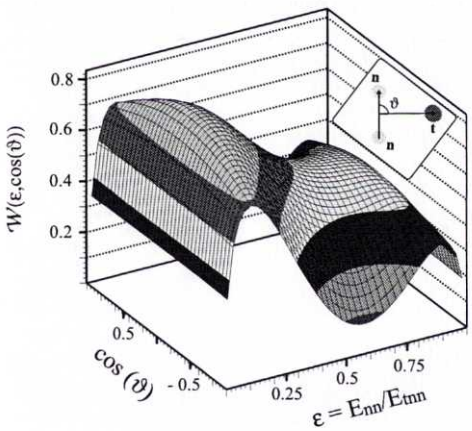

Figure 5.13: *Two dimensional plot of the probability distribution $W(\varepsilon, \cos(\vartheta))$, extracted fitting the experimental distributions using Eq. A.6. The inset sketches the used coordinate system ($t-nn$).*

The experimental distributions for the variables ε and ϑ in the two Jacobi systems are shown in Fig. 5, Paper IV and Fig. 2, Paper V. From these distributions the weights of all the partial waves in the final state (with hypermomentum K = 0,2 and $l_{x,y} \leq 1$) were determined by fitting the data using Eq. A.6, which is described in detail in Paper IV. In short, the population of the $I^\pi = 1/2^+$ state with two neutrons in the p-shell was confirmed

and found to be dominant. Further, a good resemblance between the ^{6}He wave function and the structure of the t+n+n system was found and the differences could be explained by the decay process of the preformed ^{5}H. In addition to the mentioned distributions (Fig. 5, Paper IV and Fig. 2, Paper V), the unprojected probability distributions $\mathcal{W}(\varepsilon, \vartheta)$, shown in Figures 5.13 and 5.14, reveal several features which are not evident in the projections.

In Fig. 5.13, the angular distributions are almost flat when the relative energy ε between the two neutrons is close either to 0 or to 1. In contrast it behaves almost as $\sin^2\vartheta$ when ε is close to 0.5. This is connected with the fact that the contribution from the $K = 2$, $S = 0$ harmonic is strongly suppressed in this region and the harmonic with $K = 2$, $S = 1$ predominantly determines the correlations. Further, the probability distribution $\mathcal{W}$ along the fractional energy axis (ε) reveals two distinct peaks clearly seen in the vicinity of $\vartheta = 0$ and 180 degrees. The peaks are described mainly by the interference of the harmonics with $K = 2$, $S = 0$ and $K = 0$, $S = 0$ and reflects the dynamical correlations which have been discussed for the ^{6}He wave function in microscopic calculations [205]. In the conjugated spatial coordinates the peaks correspond to the di-neutron configuration with the two neutrons forming a cluster on one side of the triton and to the cigar-like configuration where the neutrons are separated from each other by the triton core.

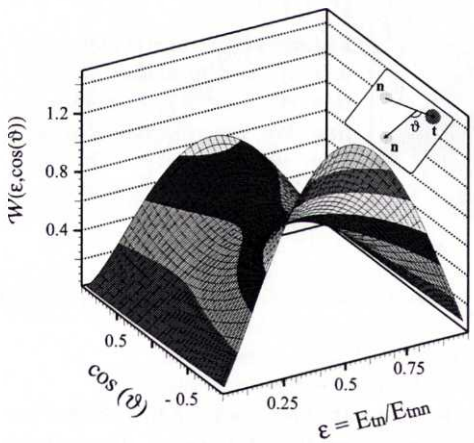

Figure 5.14: *Two dimensional plot of the probability distribution $\mathcal{W}(\varepsilon, \cos(\vartheta))$, extracted fitting the experimental distributions using Eq. A.6. The inset sketches the used coordinate system ($n - tn$).*

Most noticeable in Fig. 5.14, is again the strong n-n interaction, observed in the asymmetry of the angular distribution (ϑ), which in addition indicates a strong interference of waves with different parity.

5.6 Discussion Papers IV-V

The data presented here for the t+n system are consistent with a ^{4}H resonance state at E_R=2.67(31) MeV, and of width Γ^{obs}=3.28(23) MeV. This result is in reasonable agreement with experiments where ^{4}H has been studied in different types of nuclear reactions using the missing mass method. The ^{4}H resonance is broad and the apparent peak position in the experimental distributions depends on the reaction mechanism. Thus, a theoretical analysis is necessary to derive the resonance energy.

Further, the results - give for the first time - access to internal correlations in the ^{5}H (t+n+n) system. This information is extremely important when trying to understand the inner structure of the nucleus. The experimental results obtained indicate that the expected configuration [52, 53] for the ^{5}H ground state is strongly populated in the reaction channel analyzed here. However, narrow resonance structures were not observed. The following fact should also be taken into consideration (see also Sect. 2.3.1): ^{4}H is unstable relative to neutron emission by 2.7 MeV, and thus, ignoring the neutron pairing energy, ^{5}H would be unstable by 5.4 MeV. The pairing effects should be less pronounced for a diluted ^{5}H system compared to that for ^{6}He, thus the neutron pairing energy in ^{6}He (2.75 MeV) may be considered as an upper limit for the one in ^{5}H. The lowest value of the ^{5}H resonance, above t+n+n threshold, would therefore be 2.6 MeV. The observed peak position in the ^{5}H relative energy spectrum is only 0.5 MeV above this value and thus in good agreement with this estimate. All experimental evidence presented in Papers IV and V together with the theoretical calculations illustrated in Fig. 5.11 indicate that the observed broad resonance is mainly due to the ^{5}H ground state.

Further, the present result, taking into account the broadness of the structure, is in agreement with some earlier results [54, 200]. The reaction channel selected here can however not reproduce the narrow structure seen in [55, 56] and can therefore not shed light on its origin. Further investigations of both theoretical and experimental nature are thus needed to clarify the situation. Experiments where all the fragments are detected and precise cross section measurements together with angular and energy correlations would be very useful in order to solve the issue.

CHAPTER 6

Outlook and conclusions

In this work I have demonstrated the way of setting up, performing, analyzing and in the end presenting the outcome of an experiment. This, my contribution to the subject very neutron rich light nuclei far from stability at the rim of the nuclear chart, has hopefully been able to shed some light on the structure of the nuclei under consideration. The road is not always as straight as one might believe when reading the thesis. There are many pitfalls to escape and dead ends to wander about in before making a final conclusion, and even then, the conclusion might not be as unambiguous as wanted.

The experimental data presented here are almost entirely stemming from direct reactions in which the target nucleus above all interacts by knocking out one particle from the projectile, whereas the residual part acts as a spectator. The relatively simple reaction mechanism allows separating the consequence of the reaction itself and that of the nuclear structure, and is thus a very important tool for extracting reliable information. Further, a major part of the work is concerned with invariant mass measurements, indeed proven to be very successful, but different experimental probes are needed to get full insight in the complex structure of a nuclear system. This is actually one of the main exclusive conclusions I have made during the progress of work. *One* single experiment is absolutely not enough to extract all characteristics of a specific nucleus. Many experiments are needed *using different techniques* in order to fully uncover the secrets hidden by nature. One particular interesting case is the ^{5}H nucleus where, as discussed here, the results

from different experiments completely disagree on its inner structure. The interplay between nuclear structure and reaction mechanism has still to be fully understood, and is most probably the reason for the discrepancy. Understanding comes from putting all the detailed pieces of information together and see the image in the jigsaw puzzle. Here, theoretical studies are very important and close interaction between experimentalists and theoreticians is a necessity. Having had the good fortune to work in such environment within the Subatomic physics group in Göteborg has been very valuable and truly instructive.

Looking into the future then, what remains to be done? And what directions of research seem the most profitable to pursue?

First of all, a third and consecutive experiment would be a natural continuation of the experimental program explained here. Such an experiment was actually realized in September 2001 in addition to the previous two very successful "halo breakup" experiments with the ALADIN–LAND set up.

This time the experimental set up was improved even more, making it possible to explore regions further out from the dripline. The detection of up to five particles in the final state, in a nearly 4π geometry was feasible. In addition, a segmented CsI γ–detector was used, to provide information about electromagnetic decay channels in the break–up reactions. A liquid hydrogen target was constructed to assure reactions of purely nuclear origin, and was used together with a ΔE–E telescope detector, placed perpendicular to the target to detect scattered or knocked out protons. In addition to this, the primary beam intensity was increased by more than one order of magnitude.

The experimental data is now being analyzed and its outcome will most probably be very helpful in understanding and uncover the complicated structure of many dripline nuclei teetering on the brink of nuclear stability. Some of the more exotic reaction channels investigated will be ^{1}H(^{14}Be,2p)^{13}Li, ^{1}H(^{11}Li,2p)^{10}He, ^{1}H(^{8}He,2p)^{7}H, just to single out a few among many others.

However, a sign of warning should be raised. With the increasing complexity of the experimental set-ups in order to obtain more detailed information, the complexity of the data is drastically increased and the conclusions are getting more difficult to extract. Sometimes it is important to step aside, look back, and return to simpler experiments in order not to loose perspective.

A good example of a future experiment would be to confirm the $I^{\pi} = 1/2^{-}$ resonance state in ^{7}He in the one-neutron pick-up reaction ^{9}Be(^{6}He,^{7}He)^{8}Be, measuring the two α particles of the decaying ^{8}Be. If

performed e.g. at REX-ISOLDE using a radioactive ^{6}He beam with just a few MeV/u, thus in a totally different energy regime, an excellent complement to the experiment presented here would be accomplished. Further, this would also increase the knowledge and insight of the intricate ^{8}He system giving additional input to the theoretical problem concerning the strength of LS forces in the region.

In addition to the nucleon knock-out channels discussed in this work, cluster knock-out may also be used to reveal structural properties. In this context, the successful work by Yoshimura et al. [206] is worth mentioning, where the α-particle knockout from ^{12}C, ^{9}Be, ^{7}Li and ^{6}Li was studied. The α-cluster knock-out will provide further insight to the halo structure, where a good example would be to study the different structures of ^{6}He and ^{8}He discussed here. Further, the α-cluster knock-out will give access to extremely neutron rich resonances, such as ^{1}H(^{14}Be,pα)^{10}He, ^{1}H(^{11}Li,pα)^{7}H or ^{1}H(^{8}He,pα)4n which are just briefly investigated before.

On a larger scale, several accelerator facilities presently under construction, commissioning or being proposed or discussed worldwide (such as RIA in the United States [207], the DRIBS project at Dubna [208], the next generation ISOL facility EURISOL in Europe [209], just to name a few not previously mentioned), will without doubt, in the coming years make valuable contributions to the nuclear structure studies.

Even if we think we now know what the basic building blocks of the universe are we still have a long way to go until we can describe all the complex properties of matter. One reason for this is that we still know too little about fundamental forces and their underlying symmetries. This is especially the case with the strong force acting between quarks and between nucleons, a force that still remains a mystery. There are many questions to be asked and probably even more not yet formulated. However a few questions closely related to the subject though, could be:

- Why are protons and neutrons so much heavier than their constituents?
- In what ratios of neutrons to protons can nuclei exist? What new properties do highly unstable nuclei reveal?
- How were heavy nuclei and transuranium elements synthesized? What is the significance of unstable nuclei in this process?

Even though our understanding of nuclear structure at the driplines has increased drastically the last decade, the picture we have of the nuclei is

still to a large extent phenomenological. There is not yet any theory having a true predictive power for nuclei at the dripline, like the shell model for tightly bound nuclei. However, the availability of much increased beam intensities will allow not only to expand the knowledge about the exact location of the driplines, but also provide sufficient secondary beam intensities for detailed nuclear structure studies giving additional inputs to the theories.

Nevertheless, we are still only in the initial stages of exploring the outer parts of the nuclear landscape, and the next generations with radioactive nuclear beams will undoubtedly provide new possibilities for research with very good chances of discovering new phenomena, and other secrets lurked by nature yet too fantastic for us to imagine. To have the privilege of being not only a spectator but a participant in this process is a remarkable experience.

CHAPTER 7

Acknowledgements

During the years as a PhD student I've met many people at many different places, and you have all contributed in some way, making the journey memorable, instructive and unforgettable. Since I've had more or less two main workingplatforms, one at CTH/GU, and the other one at GSI/TU–Darmstadt, unavoidably a large number of people have been involved in my work, and I would therefore like to express my gratitude to at least a few of them.

First and most importantly I would like to thank my two supervisors in Göteborg, Björn Jonson and Göran Nyman for your enthusiasm and guidance throughout the years, something which I have indeed appreciated, and in addition for creating a very good and stimulating working environment.

I would also like to express my gratitude to Leonid Chulkov for excellent physics counseling and never-ceasing curiosity to explore unknown territories, and Haik Simon for always having solutions to all problems. Without you two this thesis would probably not have been written. Further, Mikhail Zhukov for always sharing your vast knowledge, and for pedagogical explanations concerning theoretical aspects of my work.

It's impossible with just a few single words express the full significance of Karin and Christian since we have become close friends both on- and off duty. So to both of you – THANKS for all!

Thanks to Kate for all your creative ideas, – bonus points for the cover page! – help with boring administrative paperwork and especially for always keeping the spirits high. Of course thanks to all present and former members of the group: Halina, Yulia, Maria, Marie, Natalja, Hanna, Elisabeth, Örjan, Lasse, Valter, Håkan, Kenny, Heinrich, Leif, Fredrik, Martin, Leonid, and all other short time visitors, together creating a very good–humored atmosphere.

Special thanks to Achim Richter for offering me a temporary position at the TU–Darmstadt, to Gottfried Münzenberg for doing the same at GSI and my "co–supervisor" Gerhard Schrieder for good cooperation throughout my many visits at GSI.

I would also like to thank Hans Emling and the LAND Leute, both present and previous members, Kate, Chiara, Muriel, Konstanze, Ingrid, Ushasi, Tom, Armin, Alex, Stamenko, Przemyslaw, Palit, Wawrzyniec, and Günter whom I've had the good fortune to work with at GSI, and especially my colleagues in office 3.190, Monica, Jürgen and Ivan.

On this occasion, I will take the opportunity to thank my old physics teacher from gymnasiet, Alf Ölme, you are the one who really brought me into the world of physics in the first place.

Further, thanks to all with whom I've worked when participating in different experiments, or being just friendly company at conferences and meetings whether from Stockholm, Lund, ISOLDE, Århus, Madrid, Oslo, Moscow, Tokyo, Örebro or other places: Uffe, Karsten, Hans, Henrik, Olof, Maria, Yolanda, Luis, Lola, Eugenia, Joakim, Thomas, Katarina, Håvar, Vasili, Kenta, Maggie, Andreas and many, many more.

Göteborg 2003-05-05

Mikael Meisel

APPENDICES

APPENDIX A

Jacobi coordinates and hyperspherical harmonics

A.1 Jacobi coordinates

In a three-body problem a system of three particles i, j, k with coordinates $\mathbf{r}_i$, $\mathbf{r}_j$, $\mathbf{r}_k$ in an arbitrary coordinate system are dealt with*. However in most three-body problems such a coordinate selection is not very convenient because the internal symmetry of the particles (if any) cannot be appropriately described. For this reason, it is more convenient to introduce the c.m. coordinate $\mathbf{R}$ of the three-body system and two other translationally invariant coordinates, which do not depend of the c.m. motion of the three-body system.

There are several ways of introducing two translationally invariant coordinates describing the internal motion of the particles i, j, k. One possibility is to introduce so called Jacobi coordinates, illustrated in Fig. A.1. These coordinates are often used in quantum three-body problems because the kinetic energy operator has a separated form and does not contain any mixing terms.

Two Jacobi radii, $\mathbf{x}$ and $\mathbf{y}$, can be introduced where one radius is between particles j and k, $\mathbf{x} = \mathbf{r}_j - \mathbf{r}_k$ and the other between particle i and c.m. of the selected pair, $\mathbf{y} = (\mathrm{m}_j\mathbf{r}_j + \mathrm{m}_k\mathbf{r}_k)/(\mathrm{m}_j + \mathrm{m}_k) - \mathbf{r}_i$. In addition we can introduce the hyperradius ρ, measuring the overall size of the system, and is invariant

*All particles are assumed to be spinless, a general case including spin is considered in [203].

with respect to rotations and permutation of the particles. ρ is defined as

$$\rho^2 = \mathbf{x}^2 + \mathbf{y}^2 = \rho^2(\sin^2\theta_\rho + \cos^2\theta_\rho) \tag{A.1}$$

where $\theta_\rho = \arctan(x/y)$ is the hyperangle.

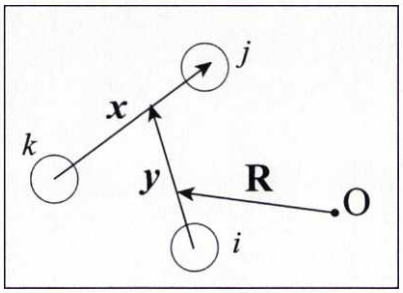

Figure A.1: *Illustration of a Jacobi coordinate system.*

In the momentum space we can introduce the corresponding Jacobi momenta $\mathbf{p}_x$, $\mathbf{p}_y$, which are conjugated to the Jacobi coordinates $\mathbf{x}$ and $\mathbf{y}$, and the Jacobi energies E_x, E_y, which are defined in analogous ways (naturally, $E_x + E_y = E$). Further, in analogy to the coordinate space we can in momentum space define the "momentum" κ and hyperangle θ_κ as

$$\kappa^2 = \mathbf{p}_x^2 + \mathbf{p}_y^2 = \kappa^2(\sin^2\theta_\kappa + \cos^2\theta_\kappa). \tag{A.2}$$

Thus a system of three particles i, j, k with fixed total energy E can be characterized by five kinematical variables, $\mathbf{\Omega}_i = (\mathbf{\Omega}_x, \mathbf{\Omega}_y, \theta_\kappa)$, where $\mathbf{\Omega}_x$ and $\mathbf{\Omega}_y$ are the directions of the respective Jacobi momenta and $\theta_\kappa = \arctan(\sqrt{E_x/E_y}) = \arctan(\sqrt{p_x/p_y})$, reflecting the energy distribution between the Jacobi subsystems[†].

By introducing the hyperradius and the hyperangle, we can make use of the hyperspherical harmonics method.

A.2 Hyperspherical harmonics

The hyperspherical harmonics (HH) formalism was introduced in 1935 by Zernike and Brinkman [210]. The formalism was then reintroduced 25 years

[†]In reality we use normalized Jacobi coordinates in both coordinate and momentum space [15].

later by Delves [203, 211] and Smith [212, 213] and has ever since proven to be a powerful tool to study few-body atomic and nuclear systems, see e.g. the reviews by Krivec [214] and Zhukov et al. [15].

A motivation for introducing HH is to reduce the N-body, ($3N$-3)-variable center-of-mass Schrödinger equation to a system of coupled ordinary differential equations in a single variable. This makes it possible to use the existing tools from the theory of Fourier series, orthogonal polynomials and the solution of systems of ordinary differential equations. In this way, many quantities appearing in the HH formulation are generally expressible through closed analytic expressions.

The HH are the eigenfunctions of the angular part of the Schrödinger equation in the six dimensional space [205],

$$\mathcal{Y}^{l_x,l_y}_{KLM} = N^{l_x,l_y}_K [\sin\theta_\rho]^{l_x} [\cos\theta_\rho]^{l_y} P^{\alpha,\beta}_n(\cos 2\theta_\rho) \left[Y_{l_x}(\hat{x}) \otimes Y_{l_y}(\hat{y})\right]_{LM} \qquad \text{(A.3)}$$

and represents a generalization of the expansion on Legendre polynomials known from two-body systems to the case of three-body systems. Here, $Y_{lm}(\hat{x})$ is the ordinary spherical harmonic function, N^{l_x,l_y}_K is a normalization constant, $P^{\alpha,\beta}_n$ are the Jacobi polynomials with $\alpha = l_x + \frac{1}{2}$ and $\beta = l_y + \frac{1}{2}$, see e.g. Ref. [215]. The additional quantum number $K = l_x + l_y + 2n$ (n = 0,1,2...) is called the hypermomentum. This is a three-body analogy to the orbital momentum in the two-body case. In this approach the centrifugal barrier of the three-body system is proportional to $(K + 3/2)(K + 5/2)/\rho^2$ corresponding to the $l(l + 1)/r^2$ factor in the two-particle case.

The transition between one set of Jacobi coordinates to another is accompanied by a change of the HH according to the formula:

$$\mathcal{Y}^{l_x,l_y}_{KLM}(\Omega_5) = \sum_{l'_x l'_y} \langle l'_x l'_y \mid l_x l_y \rangle_{KL} \mathcal{Y}^{l'_x,l'_y}_{KLM}(\Omega'_5) \qquad \text{(A.4)}$$

where $\langle ... \mid ... \rangle$ denotes the Raynal-Revai coefficients [216].

A.2.1 Some examples

In Paper IV and V, in order to determine the weights of the different partial waves in the t+n+n system from the experimental data, the method proposed in Ref. [204, 217] was used. The method is based on a fitting procedure using the HH series expansion of the amplitudes of the three-body decay. A general formulae for the approach can be found in Ref. [218].

The procedure was first to introduce a set of normalized Jacobi momentum coordinates in the projectile rest frame:

$$\mathbf{q}_{12} = (\frac{\mu_{12}}{2})^{\frac{1}{2}} \left(\frac{\mathbf{p}_1}{m_1} - \frac{\mathbf{p}_2}{m_2} \right); \tag{A.5}$$

$$\mathbf{q}_{3-12} = (\frac{\mu_{3-12}}{2})^{\frac{1}{2}} \left(\frac{\mathbf{p}_3}{m_3} - \frac{\mathbf{p}_1 + \mathbf{p}_2}{m_1 + m_2} \right)$$

where m_i, μ_{12}, μ_{3-12} and $\mathbf{p}_i$, $(i = 1, 2, 3)$ are masses, reduced masses and momenta of the particles respectively. Two different sets of Jacobi coordinates were used, **A** and **B**, see Fig. 2, Paper IV. In **A** indices 2,3 are related to neutrons and 1 to the triton, while in **B** 1,2 are related to the neutrons and 3 the triton. The total kinetic energy in the t+n+n system is then equal to $E_{tnn} = q_{12}^2 + q_{3-12}^2$. The three-body configuration can then be expressed in terms of the angle ϑ between the Jacobi momenta $\mathbf{q}_{12}$ and $\mathbf{q}_{3-12}$, by the total energy of the three-body system E_{tnn} and by the energy shared by one pair of particles $\varepsilon = q_{12}^2/E_{tnn}$.

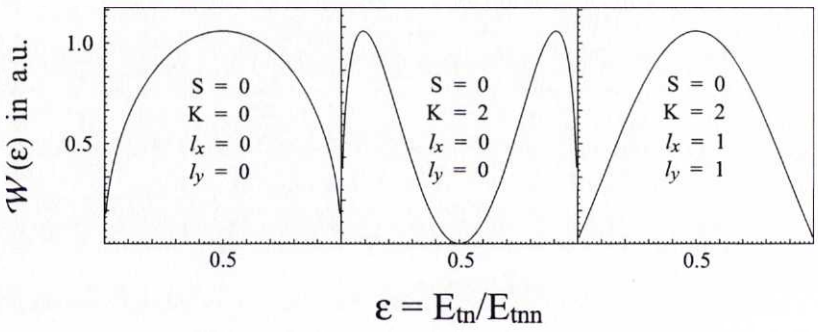

Figure A.2: *Illustration of the correlation function $\mathcal{W}(\varepsilon, \vartheta)$, (A.6) calculated solely with one amplitude, $C_{SKl_xl_y} = C_{0000}$, C_{0200}, C_{0211} from left to right respectively.*

Finally, according to [204, 217] the energy and angular correlations in the t+n+n system can be described by a probability distribution $\mathcal{W}(\varepsilon, \vartheta)$, representing the probability of finding the system in a configuration in vicinity of definite values ε and ϑ. The expansion can be characterized by a set of complex amplitudes $C_{SKl_xl_y}$ for the respective harmonics, where S is the total

spin of the two neutrons, K is the hypermomentum, and $l_{x(y)}$ are the relative angular momenta in the corresponding Jacobi coordinate system. Only the lowest terms K = 0,2 and $l_{x(y)}$ = 0,1 were here used the the expansion.

The explicit expression for the probability distribution $\mathcal{W}$ used to fit the data, valid in both Jacobi sets, has the following form

$$\mathcal{W}(\varepsilon,\vartheta) = \frac{4}{\pi}\sqrt{\varepsilon(1-\varepsilon)} \cdot \left\{ \left| C_{1211} \right|^2 8\varepsilon(1-\varepsilon)\sin^2\vartheta \right. \quad \text{(A.6)}$$
$$\left. + \left| C_{0000} - C_{0200}\, 2(2\varepsilon-1) + C_{0211}\, 4\sqrt{\varepsilon(1-\varepsilon)}\cos\vartheta \right|^2 \right\},$$

where $\mathcal{W}(\varepsilon,\vartheta)$ is normalized to unity.

The fitting procedure and its outcome is in detailed described in Paper IV. However, in order to explicitly demonstrate the shapes and characteristics of the different amplitudes, the correlation function is here calculated with one single component at a time, the result can be seen in Fig. A.2. Here the distributions are shown in configuration **A**, however the distributions in configuration **B** would have the same shapes.

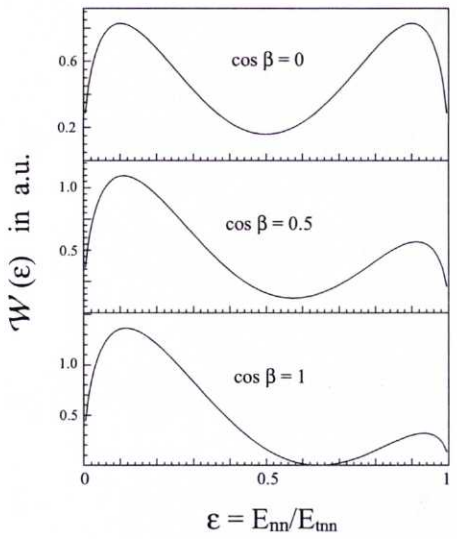

Figure A.3: *Illustration showing the influence of the phase difference (β = 90°, 60°, 0°, from top to bottom respectively) between the amplitudes C_{0000} and C_{0200} in configuration* **B**. *The correlation function $\mathcal{W}(\varepsilon,\vartheta)$, (A.6) is calculated with $|C_{0000}|^2$ = 0.25, $|C_{0200}|^2$ = 0.75 and $|C_{0211}|^2 = |C_{1211}|^2$ = 0.*

Further, in Paper IV, Fig. 5(2) an asymmetry is clearly noticeable in the experimental distribution. The origin of this asymmetry is the interference between the two amplitudes C_{0000} and C_{0200}, depending on the phase difference β between them. In order to illustrate this effect the correlation function is here calculated (see Fig. A.3) solely with the two corresponding amplitudes responsible for the asymmetry. Note that,

$$\mathcal{W} \sim \mid C_{0000} - 2(2\varepsilon - 1)C_{0200}e^{i\beta} \mid^2 \tag{A.7}$$

$$\sim \mid C_{0000} \mid^2 + \mid 2(2\varepsilon - 1)C_{0200} \mid^2 - 2C_{0000}2(2\varepsilon - 1)C_{0200}\cos\beta.$$

As can be seen in Fig. A.3 the phase difference β clearly influences the shape of the distribution, here shown in configuration **B**. The weight of the two components is here, $\mid C_{0000} \mid^2 = 0.25$ and $\mid C_{0200} \mid^2 = 0.75$.

Similar asymmetries can be seen in configuration **A** in the two distributions shown in Fig. 5(1) and Fig. 5(3) in Paper IV. Again the asymmetry is due to interference between amplitudes with different quantum numbers.

Bibliography

[1] H. A. Bethe and R. F. Bacher, Rev. Mod. Phys. **8**, 82 (1936).

[2] S. Hofmann, Eur. Phys. J. A **15**, 195 (2002).

[3] J. E. Bond and F. W. K. Firk, Nucl. Phys. A **287**, 317 (1977).

[4] L. Axelsson et al., Phys. Rev. C **54**, R1511 (1996).

[5] B. Greene, *The Elegant Universe: Superstrings, Hidden Dimensions and the Quest for the Ultimate Theory*, W. W. Norton & Company, 1999.

[6] M. S. Smith and K. E. Rehm, Annu. Rev. Nucl. Part. Sci. **51**, 91 (2001).

[7] I. Tanihata et al., Phys. Rev. Lett. **55**, 2676 (1985).

[8] J. S. Al-Khalili, I. J. Thompson, and J. A. Tostevin, Phys. Rev. C **54**, 1843 (1996).

[9] E. Arnold et al., Phys. Lett. B **197**, 311 (1987).

[10] I. Tanihata et al., Phys. Lett. B **160**, 380 (1985).

[11] I. Tanihata et al., Phys. Lett. B **206**, 592 (1988).

[12] P. G. Hansen and B. Jonson, Europhys. Lett. **4**, 409 (1987).

[13] K. Riisager, *Residence in forbidden regions*, Arhus University, 1993, Academical dissertion.

[14] A. S. Jensen and K. Riisager, Phys. Lett. B **480**, 39 (2000).

[15] M. V. Zhukov et al., Phys. Rep. **231**, 151 (1993).

[16] T. Zheng et al., Nucl. Phys. A **709**, 103 (2002).

[17] M. V. Zhukov, Nucl. Phys. A **689**, 257c (2001).

[18] P. G. Hansen and B. M. Sherrill, Nucl. Phys. A **693**, 133 (2001).

[19] B. Jonson and K. Riisager, Philos. Trans. R. Soc. London, Ser. A **356**, 2063 (1998).

[20] I. Tanihata, J. Phys. G **22**, 157 (1996).

[21] P. G. Hansen, A. S. Jensen, and B. Jonson, Annu. Rev. Nucl. Part. Sci. **45**, 591 (1995).

[22] P. Navrátil and B. R. Barrett, Phys. Rev. C **57**, 3119 (1998).

[23] H. G. Bohlen et al., Prog. Part. Nucl. Phys. **42**, 17 (1999).

[24] A. Doté and H. Horiuchi, Prog. Theo. Phys. **103**, 261 (2000).

[25] L. Chen et al., Phys. Lett. B **505**, 21 (2001).

[26] D. J. Millener, Nucl. Phys. A **693**, 394 (2001).

[27] S. Aoyama, Phys. Rev. Lett. **89**, 052501 (2002).

[28] C. S. Pieper, Eur. Phys. J. A **13**, 75 (2002).

[29] A. Ozawa, T. Kobayashi, T. Suzuki, K. Yoshida, and I. Tanihata, Phys. Rev. Lett. **84**, 5493 (2000).

[30] I. Tanihata, Nucl. Phys. A **682**, 114c (2001).

[31] T. Otsuka, R. Fujimoto, B. A. Brown, M. Honoma, and T. Mizusaki, Phys. Rev. Lett. **87**, 082502 (2001).

[32] B. A. Brown, Prog. Part. Nucl. Phys. **47**, 517 (2001).

[33] D. R. Tilley, H. R. Weller, and G. M. Hale, Nucl. Phys. A **541**, 1 (1992).

[34] D. R. Tilley et al., Nucl. Phys. A **708**, 3 (2002).

[35] M. V. Zhukov, A. A. Korsheninnikov, and M. Smedberg, Phys. Rev. C **50**, R1 (1994).

[36] K. Varga, Y. Suzuki, and Y. Ohbayasi, Phys. Rev. C **50**, 189 (1994).

[37] J. Wurzer and H. M. Hofmann, Phys. Rev. C **55**, 688 (1997).

[38] L. V. Chulkov and G. Schrieder, Z. Phys. A **359**, 231 (1997).

[39] I. Tanihata et al., Phys. Lett. B **289**, 261 (1992).

[40] M. J. G. Borge et al., Nucl. Phys. A **560**, 664 (1993).

[41] C. Gaarde et al., Nucl. Phys. A **334**, 248 (1980).

[42] L. V. Grigorenko, B. V. Danilin, V. D. Efros, N. B. Shulgina, and M. V. Zhukov, Phys. Rev. C **57**, R2099 (1998).

[43] M. Smedberg, *Probing the drip–lines through momentum distributions*, PhD thesis, Chalmers University of Technology, Göteborg University, 1998, **ISBN 91-7197-741-4**.

[44] Y. Suzuki and K. Ikeda, Phys. Rev. C **38**, 410 (1988).

[45] C. F. von Weizsäcker, Z. Phys. **96**, 431 (1935).

[46] K. S. Krane, *Introductory Nuclear Physics*, John Wiley and Sons, New York, 1988.

[47] A. A. Ogloblin and Y. E. Penionzhkevich, Very Neutron-Rich Very Light Nuclei, in *Treatise on Heavy-Ion Science*, edited by D. A. Bromley, volume 8, pages 261–360, Plenum Press NY, 1989.

[48] A. A. Ogloblin, Z. Phys. A **351**, 355 (1995).

[49] W. von Oertzen et al., Nucl. Phys. A **588**, 129c (1995).

[50] C. H. Blanchard and R. G. Winter, Phys. Rev. **107**, 774 (1964).

[51] E. G. Adelberger, A. B. McDonald, T. A. Tombrello, F. S. Dietrich, and A. V. Nero, Phys. Lett. B **25**, 595 (1967).

[52] N. B. Shulgina, B. V. Danilin, L. V. Grigorenko, M. V. Zhukov, and J. M. Bang, Phys. Rev. C **62**, 014312 (2000).

[53] P. Descouvemont and A. Kharbach, Phys. Rev. C **63**, 027001 (2001).

[54] M. G. Gornov et al., *LII meeting on Nuclear Spectroscopy and Nuclear Structure, Moscow, Russia*, in *Book of Abstracts*, page 70, 2002.

[55] G. M. Ter-Akopian, *VII International School Seminar, Dubna, Russia*, in *Book of Abstracts*, page 87, 2002.

[56] A. A. Korsheninnikov et al., Phys. Rev. Lett. **87**, 092501 (2001).

[57] F. M. Marqués et al., Phys. Rev. C **65**, 044006 (2002).

[58] A. A. Korsheninnikov et al., Phys. Rev. Lett. **90**, 082501 (2003).

[59] V. I. Goldansky, Nucl. Phys. **19**, 482 (1960).

[60] L. V. Grigorenko, I. G. Mukha, and M. V. Zhukov, Nucl. Phys. A **713**, 372 (2003).

[61] L. V. Grigorenko, I. G. Mukha, and M. V. Zhukov, Nucl. Phys. A **714**, 425 (2003).

[62] D. V. Aleksandrov et al., Yad. Fiz. **39**, 513 (1984).

[63] R. W. Gurney and E. U. Condon, Nature **122**, 439 (1928).

[64] G. Gamov, Z. Phys. **51**, 204 (1928).

[65] J. D. Crockcroft and E. T. S. Walton, Proc. Royal. Soc. A **136**, 619 (1932).

[66] The Nobel Foundation, http://www.nobel.se/, [Accessed Feb. 13, 2003].

[67] Ernest Lawrence and the cyclotron: AIP History Center Web Exhibit, http://www.aip.org/history/lawrence /larger-image-page/epa-13.htm, [Accessed April. 10, 2003].

[68] H. Geissel, G. Münzenberg, and K. Riisager, Annu. Rev. Nucl. Part. Sci. **45**, 163 (1995).

[69] A. C. Mueller et al., Nuclear structure under extreme conditions of isospin, mass, spin and temperature, in *NUPECC Report*, Dec. 1997.

[70] J. Benlliure, T. Enqvist, A. R. Junghans, V. Riccardi, and K.-H. Schmidt, Possibilities for the Production of Non-Stable Isotopes, in *XXXVII Int. Winter meeting on Nuclear Physics, Bormio, Italy*, 1999.

[71] J. Äystö and V. Rubchenya, Eur. Phys. J. A **13**, 109 (2002).

[72] A. Watson, Science **286**, 28 (1999).

[73] H. L. Ravn and B. Allardyce, On-Line Mass Separators, in *Treatise on Heavy Ion Science*, edited by D. Allan Bromley, volume 8, page 363, Plenum Publishing Corp, 1989.

[74] R. Kirchner, Nucl. Instr. Meth. B **70**, 186 (1992).

[75] H. O. U. Fynbo, *Beta–delayed particle emission from the dripline nuclei* ^{11}Li, ^{31}Ar *and* ^{9}C, PhD thesis, University of Aarhus, 1999.

[76] U. C. Bergmann, *Exotic Decays of Nuclei at the Limits of Existence*, PhD thesis, University of Aarhus, 2000.

[77] F. J. C. Wenander, *Charge Breeding and Production of Multiply Charged Ions in EBIS*, PhD thesis, Chalmers University of Technology and Göteborg University, 2001, **ISBN 91-7291-009-7**.

[78] GSI Homepage, http://www.gsi.de, [Accessed Mar, 13, 2003].

[79] K. D. Hildenbrand, Phys. Bull. **June**, 270 (1977).

[80] Accelerator System Homepage, http://www.gsi.de/gsi.accelerator.html, [Accessed Feb. 13, 2003].

[81] H. Geissel et al., Nucl. Instr. Meth. B **70**, 286 (1992).

[82] FRS Homepage, http://www-wnt.gsi.de/frs/toppage.html, [Accessed Mar, 13, 2003].

[83] ESR Homepage, http://www.gsi.de/accelerator/esr.p17.html, [Accessed Mar, 13, 2003].

[84] Ship Homepage, http://www.gsi.de/ship/home.html, [Accessed Feb. 13, 2003].

[85] Biophysics Homepage, http://www-aix.gsi.de/~bio/home.html, [Accessed Mar, 13, 2003].

[86] K.-D. Groß, H. H. Gutbrod, W. F. Henning, and J. Reiß, editors, *An International Accelerator Facility for Beams of Ions and Antiprotons - Conceptual Design Report*, GSI, Darmstadt, Germany, 2001.

[87] F. Humbert, *Kinematisch vollständige Messung der Aufbruchreaktionen von leichten, neutronenreichen Kernen am Beispiel des Halokerns ^{11}Li*, PhD thesis, Technische Universität Darmstadt, 1995.

[88] T. Nilsson, *Excursions along the Drip line*, PhD thesis, Chalmers University of Technology and Göteborg University, 1995, **ISBN 91-7197-215-3**.

[89] M. Zinser, *Aufbruchreaktionen hochenergetischer Neutron-Halo-Kerne*, PhD thesis, Universität Mainz, 1996.

[90] H. Simon, *Aufbruchreaktionen der Halokerne ^{11}Li und ^{14}Be bei relativistischen Energien*, PhD thesis, Technische Universität Darmstadt, 1998.

[91] B. Eberlein, *Aufbruchreaktionen des Halo–Kerns ^{8}He*, PhD thesis, Universität Mainz, 1998.

[92] W. Dostal, *Spektroskopie des Halo–Kerns ^{6}He*, PhD thesis, Universität Mainz, 1999.

[93] ALADIN–Collaboration, GSI Ann. Rep. , p. 292 (1989).

[94] ALADIN Homepage, http://www-kp3.gsi.de/www/kp3/aladinhome.html, [Accessed Mar, 13, 2003].

[95] T. Blaich et al., Nucl. Instr. Meth. A **314**, 136 (1992).

[96] LAND Homepage, http://www-land.gsi.de/a_new_land/index.html, [Accessed Feb. 13, 2003].

[97] H. Stelzer, Nucl. Instr. Meth. A **310**, 103 (1991).

[98] G. Charpak and F. Sauli, Nucl. Instr. Meth. **162**, 405 (1979).

[99] W. R. Leo, *Techniques for Nuclear and Particle Physics Experiments*, Springer–Verlag Berlin Heidelberg, 1987.

[100] G. F. Knoll, *Radiation Detection and Measurement*, John Wiley & Sons, Inc., 1979.

[101] J. Cub, K. Grimm, and E. Zude, GSI Ann. Rep. , p. 275 (1994).

[102] M. Zinser et al., Nucl. Phys. A **619**, 151 (1997).

[103] A. Leistenschneider, *Entwicklung eines Schauererkennungsalgorithmus für den Neutronendetektor-LAND*, Universität Frankfurt, 1997, Diploma Thesis.

[104] CERN Program Library entry Q121, PAW–Physics Analysis Workstation, CERN, Geneva, Switzerland, 1993.

[105] T. Blaich et al., GSI Ann. Rep. , p. 311 (1989).

[106] Y. Leifels, *Neutronenfluß in Schwerionenstöß en bei 400 AMeV im System Au+Au*, PhD thesis, University Bochum, 1993.

[107] R. Serber, Phys. Rev. **72**, 1008 (1947).

[108] J. J. Sakurai, *Modern Quantum Mechanics*, Addison Wesley, 1994, Revised edition.

[109] C. A. Bertulani, M. S. Hussein, and G. Münzenberg, *Physics of Radioactive Beams*, Nova Science Publishers, Inc. Huntington, New York, 2001.

[110] G. F. Bertsch, K. Hencken, and H. Esbensen, Phys. Rev. C **57**, 1366 (1998).

[111] R. J. Glauber, Phys. Rev. **99**, 1515 (1955).

[112] G. F. Bertsch, B. A. Brown, and H. Sagawa, Phys. Rev. C **39**, 1154 (1989).

[113] G. F. Bertsch, B. A. Brown, and H. Sagawa, Phys. Rev. C **42**, 758 (1990).

[114] Y. L. Parfenova, M. V. Zhukov, and J. S. Vaagen, Phys. Rev. C **62**, 044602 (2000).

[115] Y. L. Parfenova and M. V. Zhukov, Eur. Phys. J. A **12**, 191 (2001).

[116] R. Shyam and H. Lenske, Phys. Rev. C **57**, 2427 (1998).

[117] S. N. Ershov, B. V. Danilin, and J. S. Vaagen, Phys. Rev. C **62**, R041001 (2000).

[118] A. Bonaccorso and D. M. Brink, Phys. Rev. C **58**, 2864 (1998).

[119] F. M. Nunes and I. J. Thompson, Phys. Rev. C **59**, 2652 (1999).

[120] Y. Ogawa, K. Yabana, and Y. Suzuki, Nucl. Phys. A **543**, 722 (1992).

[121] T. Kobayashi et al., Phys. Lett. B **232**, 51 (1989).

[122] H. H. Heckman and P. J. Lindstrom, Phys. Rev. Lett. **37**, 56 (1976).

[123] ESA Hubble Information Centre, http://sci.eas.int/hubble/, [Accessed Mar. 04, 2003].

[124] A. Winther and K. Alder, Nucl. Phys. A **319**, 518 (1979).

[125] T. Glasmacher, Annu. Rev. Nucl. Part. Sci. **48**, 1 (1998).

[126] T. Nakamura, *Coulomb Excitation of* ^{11}Be, PhD thesis, University of Tokyo, 1995.

[127] C. F. von Weizsäcker, Z. Phys. **88**, 612 (1934).

[128] E. J. Williams, Phys. Rev. **45**, 729 (1934).

[129] C. A. Bertlulani, G. Baur, and M. S. Hussein, Nucl. Phys. A **526**, 751 (1991).

[130] C. Forssén, *On the few-body character of light exotic nuclei – analytical studies of electromagnetic processes involving loosely bound systems*, PhD thesis, Chalmers University of Technology and Göteborg University, 2003, **ISBN 91-7291-260-X**.

[131] C. A. Bertulani and G. Baur, Phys. Rep. **163**, 300 (1988).

[132] J. R. Oppenheimer, Phys. Rev. **47**, 845 (1935).

[133] C. J. Mullin and E. Guth, Phys. Rev. **82**, 141 (1951).

[134] D. J. Millener, J. W. Olness, E. K. Warburton, and S. S. Hanna, Phys. Rev. C **28**, 497 (1983).

[135] K. Ieki et al., Phys. Rev. Lett. **70**, 730 (1993).

[136] D. Sackett et al., Phys. Rev. C **48**, 118 (1993).

[137] S. Shimoura et al., Phys. Lett. B **348**, 29 (1995).

[138] T. Nakamura et al., Phys. Lett. B **331**, 296 (1994).

[139] M. Labiche et al., Phys. Rev. Lett. **86**, 600 (2001).

[140] T. Nakamura et al., Phys. Rev. Lett. **83**, 1112 (1999).

[141] T. Aumann et al., Phys. Rev. C **59**, 1252 (1999).

[142] N. A. Orr, Nucl. Phys. A **616**, 155c (1997).

[143] K. Markenroth, *Exploring the Exotic - Experimental investigation far from stability*, PhD thesis, Chalmers University of Technology and Göteborg University, 2001, **ISBN 91-7291-070-4**.

[144] L. Axelsson, *Exotic Nuclei – experimental studies of nuclear structure*, PhD thesis, Chalmers University of Technology and Göteborg University, 1999, **ISBN 91-628-3933-0**.

[145] A. S. Goldhaber and H. H. Heckman, Annu. Rev. Nucl. Part. Sci. **28**, 161 (1978).

[146] I. Tanihata, Prog. Part. Nucl. Phys. **35**, 505 (1995).

[147] T. Kobayashi et al., Phys. Rev. Lett. **60**, 2599 (1988).

[148] C. A. Bertulani and K. W. McVoy, Phys. Rev. C **46**, 2638 (1992).

[149] H. Simon et al., Phys. Rev. Lett. **83**, 496 (1999).

[150] P. G. Hansen, Phys. Rev. Lett. **77**, 1016 (1996).

[151] S. Grévy et al., Nucl. Phys. A **650**, 47 (1999).

[152] A. R. Erwin, R. March, D. Walker, and E. West, Phys. Rev. Lett. **6**, 628 (1961).

[153] B. R. Martin and G. Shaw, *Particle Physics*, John Wiley & Sons, Inc., West Sussex, England, 1997.

[154] G. Breit and E. Wigner, Phys. Rev. **49**, 519 (1936).

[155] T. Kobayashi, Projectile fragmentation of exotic nuclear beams, in *Proc. of 3rd Int. Conf. on Radioactive Beams*, edited by D. J. Morrisey, pages 169–178, East Lansing, 1993.

[156] A. M. Lane and R. G. Thomas, Rev. Mod. Phys. **30**, 257 (1958).

[157] D. Aleksandrov et al., Nucl. Phys. A **633**, 234 (1998).

[158] K. Siegbahn, *Alpha-, beta- and gamma-ray spectroscopy*, volume 2, Noth-Holland, 4 edition, 1974.

[159] L. C. Biedenharn and M. E. Rose, Rev. Mod. Phys. **25**, 729 (1953).

[160] L. V. Chulkov et al., Phys. Rev. Lett. **79**, 201 (1997).

[161] G. L. Morgan and R. L. Walter, Phys. Rev. **68**, 1114 (1968).

[162] E. Garrido, D. V. Fedorov, and A. S. Jensen, Phys. Rev. C **58**, R2655 (1998).

[163] R. H. Dalitz, Philos. Mag. **44**, 1068 (1953).

[164] H. O. U. Fynbo et al., Mechanism of the three-body deacy of ^{12}C (12.71 MeV), Submitted to Phys. Rev. Lett.

[165] E. L. Berger, R. Singer, G. H. Thomas, and T. Kafka, Phys. Rev. D. **15**, 206 (1977).

[166] G. Jancso et al., Nucl. Phys. B **124**, 1 (1977).

[167] D. Drijard, H. G. Fischer, and T. Nakada, Nucl. Instr. Meth. **225**, 367 (1984).

[168] J. Pochodzalla et al., Phys. Rev. C **35**, 1695 (1987).

[169] C. Forssén, B. Jonson, and M. V. Zhukov, Nucl. Phys. A **673**, 143 (2000).

[170] L. V. Chulkov, Nuovo. Cim. A **111**, 791 (1998).

[171] W. A. Zajc et al., Phys. Rev. C **29**, 2173 (1984).

[172] F. M. Marqués et al., Phys. Lett. B **476**, 219 (2000).

[173] R. Hanbury-Brown and R. Q. Twiss, Philos. Mag. **45**, 663 (1954).

[174] D. H. Boal, C.-K. Gelbke, and B. K. Jennings, Rev. Mod. Phys. **62**, 553 (1990).

[175] A. A. Korsheninnikov et al., Phys. Rev. Lett. **82**, 3581 (1999).

[176] H. G. Bohlen et al., Phys. Rev. C **64**, 024312 (2001).

[177] M. G. Gornov et al., Bull. Rus. Acad. Sci. Phys. **62**, 1781 (1998).

[178] W. A. Friedman, Phys. Rev. C **27**, 569 (1983).

[179] J.-L. Lecouey, *Étude des systèmes non liés* ^{16}B *et* ^{13}Be, PhD thesis, Université de Caen / Basse–Normandie, 2002.

[180] R. B. Wiringa, Nucl. Phys. A **631**, 70c (1998).

[181] R. B. Wiringa, S. C. Pieper, J. Carlson, and V. R. Pandharipande, Phys. Rev. C **62**, 014001 (2000).

[182] N. A. F. M. Poppelier, A. A. Wolters, and P. W. M. Glaudemans, Z. Phys. A **346**, 11 (1993).

[183] D. V. Aleksandrov et al., Yad. Fiz. **35**, 277 (1982).

[184] A. V. Belozerov et al., Bull. Rus. Acad. Sci. Phys. **52**, 94 (1988).

[185] A. A. Korsheninnikov et al., Phys. Lett. B **316**, 38 (1993).

[186] Y. Iwata et al., Phys. Rev. C **62**, 064311 (2000).

[187] S. A. Goncharov and A. A. Korsheninnikov, Europhys. Lett. **30**, 13 (1995).

[188] A. Bohr and B. R. Mottelson, *Nuclear structure vol I*, W. A. Benjamin, inc., 1975.

[189] D. Aleksandrov et al., Nucl. Phys. A **669**, 51 (2000).

[190] C. A. Bertulani and H. Sagawa, Nucl. Phys. A **588**, 667 (1995).

[191] R. Wolski et al., Nucl. Phys. A **701**, 29c (2002).

[192] F. Ajzenberg-Selove, Nucl. Phys. A **490**, 1 (1988).

[193] S. Aoyama, Phys. Rev. C **59**, 531 (1999).

[194] A. Csótó and G. M. Hale, Phys. Rev. C **55**, 536 (1997).

[195] B. V. Danilin, M. V. Zhukov, A. A. Korsheninnikov, and L. V. Chulkov, Sov. J. Nucl. Phys. **53**, 45 (1991).

[196] M. Zinser et al., Phys. Rev. Lett. **75**, 1719 (1995).

[197] T. W. Phillips, B. L. Berman, and J. D. Seagrave, Phys. Rev. C **22**, 384 (1980).

[198] V. D. Efros and H. Oberhummer, Phys. Rev. C **54**, 1485 (1996).

[199] B. M. K. Nefkens, Phys. Rev. Lett. **10**, 55 (1963).

[200] D. V. Aleksandrov, E. Y. Nikolsky, B. G. Novatsky, and D. N. Stepanov, Investigation of the superheavy hydrogen isotopes via exotic reactions with ^{6}He and ^{6}Li ions, in *Proc. Intern. Conf. on Exotic Nuclei and Atomic Masses (ENAM-95)*, edited by M. de Saint Simon and O. Sorlin, pages 329–330, Arles, France, 1995.

[201] P. G. Young, R. H. Stokes, and G. G. Ohlsen, Phys. Rev. **173**, 949 (1968).

[202] G. M. Ter-Akopian et al., Hydrogen-4 and Hydrogen-5 from t+t and t+d transfer reactions studied with a 57.5-MeV triton beam, in *International Nuclear Physics Conference INPC 2001*, edited by E. Norman, L. Schroeder, and G. Wozniak, pages 920–924, Berkeley, California, 2001.

[203] L. M. Delves, Nucl. Phys. **20**, 275 (1960).

[204] O. V. Bochkarev et al., Nucl. Phys. A **505**, 275 (1989).

[205] B. V. Danilin, I. J. Thompson, J. S. Vaagen, and M. V. Zhukov, Nucl. Phys. A **632**, 383 (1998).

[206] T. Yoshimura et al., Nucl. Phys. A **641**, 3 (1998).

[207] ISOL Task Force Information, http://srfsrv.JLab.org/ISOL/, [Accessed April. 25, 2003].

[208] DRIBS Home Page, http://159.93.28.88/dribs/home.html, [Accessed April. 25, 2003].

[209] EURISOL main page, http://www.ganil.fr/eurisol/, [Accessed April. 25, 2003].

[210] F. Zernike and H. C. Brinkman, Proc. Kon. Ned. Akad. Wettensch. **38**, 161 (1935).

[211] L. M. Delves, Nucl. Phys. **9**, 391 (1959).

[212] F. T. Smith, Phys. Rev. **120**, 1058 (1960).

[213] F. T. Smith, J. Math. Phys. **3**, 735 (1962).

[214] R. Krivec, Few-Body Systems **25**, 199 (1998).

[215] L. Råde and B. Westergren, *BETA – Mathematics Handbook for Science and Engineering*, Studentlitteratur, Lund, 1998.

[216] J. Raynal and J. Revai, Nuovo Cimento A **68**, 612 (1970).

[217] B. V. Danilin, M. V. Zhukov, A. A. Korsheninnikov, L. V. Chulkov, and V. D. Efros, Yad. Fiz. **46**, 427 (1987).

[218] A. A. Korsheninnikov, Yad. Fiz. **52**, 1304 (1990).

På grund av upphovsrättsliga skäl kan vissa ingående delarbeten ej publiceras här.
För en fullständig lista av ingående delarbeten, se avhandlingens början.

Due to copyright law limitations, certain papers may not be published here.
For a complete list of papers, see the beginning of the dissertation.

GÖTEBORGS UNIVERSITET

GÖTEBORG
UNIVERSITY

Faculty of Science

ISBN 91-628-5688-X